Received: 6 August 2020 | Revised: 12 November 2020 | Accepted: 15 November 2020

DOI: 10.1111/bre.12532

RESEARCH ARTICLE

Basin Research | IAS EAGE | WILEY

# The formation and implications of giant blocks and fluid escape structures in submarine lateral spreads

**Nan Wu**[1] | **Christopher A.-L. Jackson**[1] | **Howard D. Johnson**[1] | **David M. Hodgson**[2] | **Michael A. Clare**[3] | **Harya D. Nugraha**[1] | **Wei Li**[4]

[1]Basins Research Group (BRG), Department of Earth Science & Engineering, Imperial College, London, United Kingdom

[2]School of Earth and Environment, University of Leeds, Leeds, United Kingdom

[3]National Oceanography Centre, Southampton, United Kingdom

[4]South China Sea Institute of Oceanology, Chinese Academy of Sciences, Guangzhou, China

**Correspondence**
Nan Wu, Basins Research Group (BRG), Department of Earth Science & Engineering, Imperial College, Prince Consort Road, London, SW7 2BP, United Kingdom.
Email: n.wu16@imperial.ac.uk

**Funding information**
Natural Environment Research Council; China Scholarship Council

## Abstract

Lateral spread and submarine creep are processes that occur near the headwalls of both terrestrial landslides and submarine mass-transport complexes (MTCs). Both submarine creep and spread deposits may contain giant (km-scale) coherent blocks, but their transport processes remain poorly constrained. Here we use seismic reflection data to determine the geometry, scale, and origin of a Late Miocene mass-transport complex (MTC) located in the Kangaroo Syncline, offshore NW Australia. We show that this large remobilised mass of carbonate ooze is ca. 170–300 m thick and covers an area of at least 1,050 km$^2$. The deposit is defined internally by two distinct seismic facies: (a) large, upward-tapering blocks (210–300 m thick, 170–210 m wide and 800–1,200 m long) with negligible internal deformation, which decrease in height and spacing along the transport direction (identical, but in situ, seismic facies forms undeformed slope material immediately updip of the deposit headwall); and (b) troughs (160–260 m thick, 190–230 m wide and 800–1,200 m long) comprising moderately deformed strata, which contain 'v'-shaped, pipe-like structures that extend upwards from the inferred basal shear surface to the top surface. The lack of deformation within the blocks, and their correlation to adjacent in situ deposits, suggests they underwent limited transport (ca. 50 m–70 m). The relatively high degree of deformation within the intervening troughs is attributed to the vertical expulsion of fluids and sediment during hydraulic failure of the sediment mass. We present a hydraulic failure model that invokes evacuation of the lower slope by a precursor MTC and which formed the space to trigger the lateral spread. Our study also provides new insights into the genesis and rheology of subaqueous lateral spreads. The genetic links identified between mass wasting and spatially focused fluid flow, as well as disturbing the deep seafloor, indicate that submarine landslides may also create important deep-sea biodiversity hotspots.

**KEYWORDS**

Australia, Exmouth Plateau, geohazard, mass-transport complex (MTC), NW Shelf, slope failure, spread, submarine landslide

## 1 | INTRODUCTION

Mass-transport complex (MTC) is a broad term typically used to describe slope failure deposits resulting from creep, spread, slide, slump and debris flow processes (Figure 1; Nemec, 1990; Varnes, 1978). MTCs are responsible for transporting large volumes of sediments from basin margins to the adjacent basin floor, often during single catastrophic events (e.g. Posamentier & Martinsen, 2011). Because of their size, the generation and emplacement of MTCs play a key role in shaping and controlling the stratigraphic evolution of continental margins around the world (Posamentier & Martinsen, 2011). MTCs can initiate and translate over very low-angle seafloors by hydroplaning with sediments in the overlying failure mass partly or fully disaggregated to form a genetically related debris flow (De Blasio & Elverhoi, 2011). Partial disaggregation can result in the formation and emplacement of relatively coherent, largely undeformed blocks (Alves, 2015; Jackson, 2011; Li et al., 2016; Micallef et al., 2007) that may trigger tsunamis (Tappin, 2010), can damage or destroy seafloor infrastructure (Masson et al., 2006; Urlaub et al., 2013), be a precursor for subsequent slope failure events (i.e. Lee & Chough, 2001; Li et al., 2016) or increase the slope stability by reducing gravitational potential (Shillington et al., 2012). More specifically, the risks to seafloor infrastructure, and the tsunamogenic potential are dependent on the degree and rate of landslide disaggregation, the volume and strength of the failed mass and the speed and movement direction (e.g. Dutta & Hawlader, 2019; Randolph & White, 2012; Watts et al., 2005; Zakeri, 2009; Zhu & Randolph, 2010). For instance, highly mobile, yet relatively thin debris flows have toppled oil and gas platforms, and ruptured pipelines in the Gulf of Mexico (e.g. Chaytor et al., 2020). Conversely, much larger, deep-seated (i.e. relatively thick) and yet limited run-out MTCs triggered by the 2011 Tōhoku-Oki earthquake ($M_w$ 9.1) caused no discernable damage to seafloor telecommunication cables (e.g. Pope et al., 2017; Strasser et al., 2013). Therefore, differentiating the nature of slope failure processes is a key element in assessing their risk to coastal communities and critical seafloor infrastructure.

Submarine creep (or 'spreading') and lateral spreading are gravity-driven processes that occur near the headwall area of sediment failure in marine (syn.: 'submarine spread') and terrestrial (landslides) settings, respectively (Figure 1). Submarine creep is defined as a slow, gravity-driven, downslope motion or post- or syn-depositional deformation of a sediment mass (Nemec, 1990; Silva & Booth, 1984). The deposits of submarine creep may contain giant coherent blocks that are up to c. 300 m high and c. 4 km wide (e.g. Li et al., 2016).

Subaqueous spread (also known as gravitational spreading and lateral spreading; Savage & Varnes, 1987; Varnes, 1978) is another type of gravity-induced failure. First defined in terrestrial settings as 'lateral spreading', this type of failure is initiated by subsurface liquefaction and the formation of an intra-stratal weak zone, above which the failed mass translates (Varnes, 1978). Commonly, these masses are stretched and broken up into internally coherent blocks (Figure 1). A key characteristic of spreads is that they can occur above a very gently-dipping (ca. <1°) failure surface (Cruden & Varnes, 1996; Micallef et al., 2007). A subaqueous spread can have a lateral displacement of only a few tens of metres (Micallef et al., 2007). Despite this limited displacement, onshore analogues indicate that the emplacement of spread-related blocks can be extremely hazardous. For example, a spread and its associated debris occurred in Palu, Indonesia, following an earthquake in September 2018, leaving >2000 people dead and ca. 1,300 people missing (Bradley et al., 2019; Watkinson & Hall, 2019). Subaqueous spread-related deposits have received less attention than their terrestrial counterparts, despite 3D seismic reflection data being an excellent tool to resolve the external and internal geometry, and origin of this particular type of submarine landslide (Micallef et al., 2007). Although the deposits of submarine creep and spread have similar external geometries and internal seismic facies, they are different failure process and are typically not considered part of a continuum; that is, creep would not transform into spread, or vice versa.

Many landslide hazard assessments are based solely on plan-view imaging using multibeam bathymetric surveys (e.g. Geertsema et al., 2018). While incredibly valuable, such surveys lack the subsurface information required to identify and diagnose the style and depth of landslide failure, and the nature of internal deformation (Clare et al., 2019). Here we demonstrate the value of high resolution 2D and 3D seismic reflection data to complement and advance modern seafloor studies of MTCs. Our aim is to evaluate the morphology, internal structure, kinematics, origin and geohazard risk of a large submarine MTC using a high-quality, 3D and 2D seismic reflection dataset from the NW Shelf, offshore Australia. Using these data, we can quantify the height and spacing of the contained

**Highlights**

- We present a hydraulic failure model that accounts for the styles of deformation process associated with blocks.
- We provide a new hydraulic failure model account for subaqueous lateral spreads.
- The fluid flow associated with MTCs may create deep-sea biodiversity hotspots.

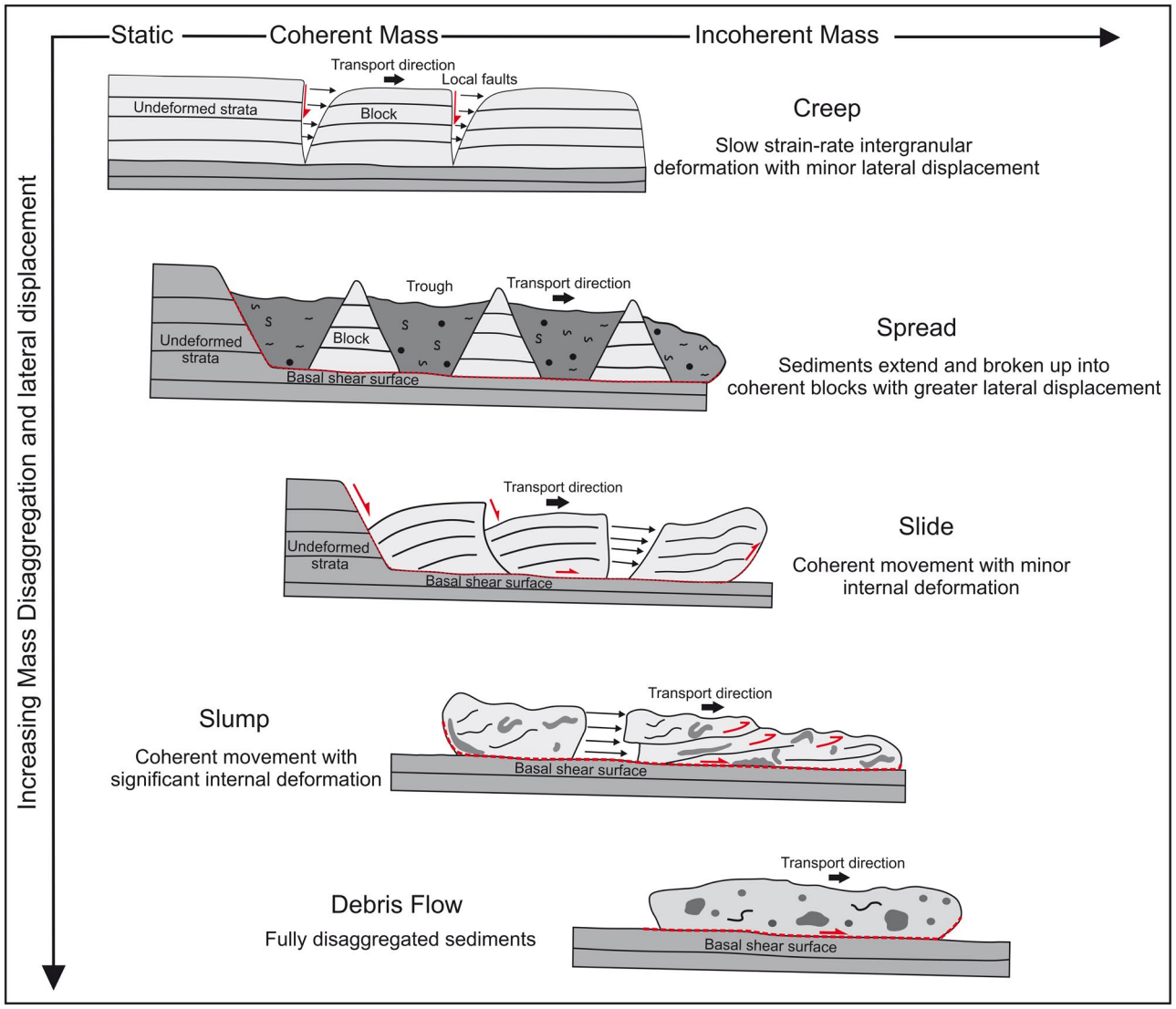


**FIGURE 1** Schematic diagram showing the classification of mass-transport complexes adopted in this study (modified from Nemec, 1990; Posamentier & Martinsen, 2011; Scarselli et al., 2013)

blocks, while a detailed kinematic analysis of intra-MTC structures allows the transport direction to be determined. This present study also aims to offer a better understanding of spread initiation, translation and deposition, which will help to build a more comprehensive model for submarine mass failures and to help understand, and hence inform mitigation of the associated geohazard risk.

## 2 | GEOLOGICAL SETTING

The Exmouth Plateau is located offshore NW Australia, ca. 900 km south of the tectonically active boundary between the Australian and Eurasian tectonic plates (Figure 2a,b; Hengesh et al., 2012, 2013). The Exmouth Plateau is ca. 600 km long and ca. 350 km wide, and is presently located in water depths of 1,100–5,000 m (Exon et al., 1992; Falvey & Veevers, 1974; Hengesh et al., 2013; Figure 2a). This study focuses on the Upper Miocene to Holocene passive margin mega-sequence (Figure 2c). This interval records the relatively slow deposition (ca. 0.02 mm/yr) of very fine-grained carbonate in bathyal (200–2,000 m) water depths (Exon et al., 1992; Haq et al., 1992; Maher & Thompson, 1999). Cores from Ocean Drilling Program (ODP) wells 762 and 763 have established that the dominant lithology in this interval is nannofossil-rich carbonate ooze (Boyd et al., 1993; Exon et al., 1992; Haq et al., 1992). These deposits are characterised by high porosities (ca. 70%) and high water saturations (ca. 40%), and by an overall low strength profile (<20kPa; von Rad and Haq, 1992; see figure 5 from Hengesh et al., 2012). These physical properties increase the slope instability and related geohazard risk of the Exmouth Plateau area. Prolonged slope instability is recorded in the presence of large

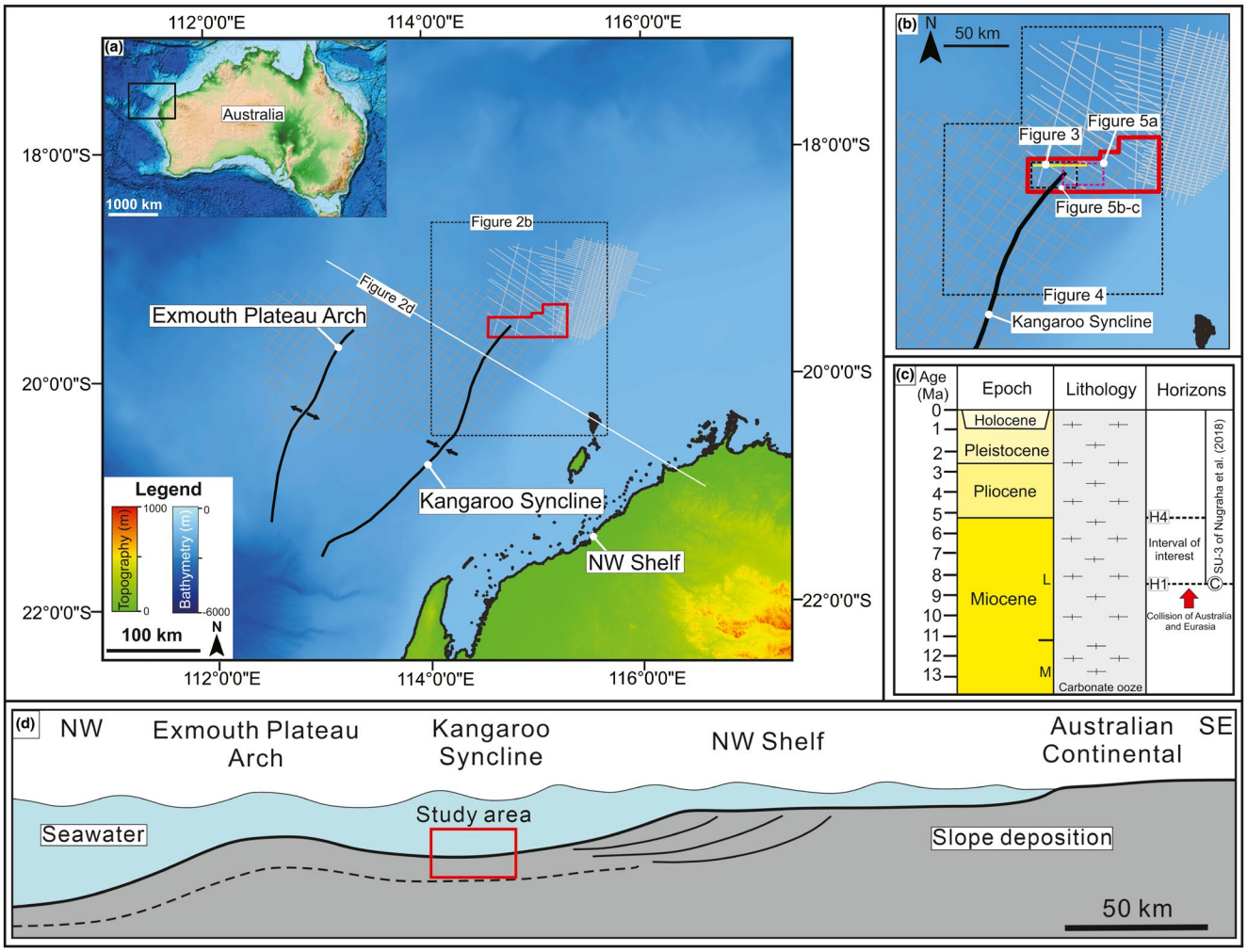


**FIGURE 2** (a) Regional map of the study area showing the location of the Exmouth Plateau Arch, Kangaroo Syncline. The white and grey lines represent 2D seismic reflection data, and the red polygon represents the location of 3D seismic reflection dataset. Shaded relief GEBCO_2014 bathymetry map downloaded from https://www.ngdc.noaa.gov/maps/autogrid/; (b) location map of the figures demonstrated in this study; (c) Stratigraphy column and the major tectonic event of the study interval; (d) Sketch map of the regional structures crossing the study area, showing the modern depositional systems, adapted from Nugraha et al. (2018)

(e.g. ca. 500 km$^3$ Gorgon slide; Hengesh et al., 2012), stacked, slope-to-basin floor MTCs in the upper part (i.e. post-Oligocene) of the passive margin mega-sequence (Hengesh et al., 2012; Nugraha et al., 2019; Nugraha et al., 2018; Scarselli et al., 2013). The study area is located in the axis of the Kangaroo Syncline, between the Exmouth Plateau to the west and the NW Shelf to the east (Figure 2a and d). The stratigraphic interval under investigation extends upwards from Horizon H1 (base) to the seafloor (top) (Figures 2c and 3a-c). Horizon H1 (Figure 3b) is a regionally mappable unconformity that defines the base of the Late Miocene, and which records collision of the Australian and Eurasian plates (Boyd et al., 1993; Hull & Griffiths, 2002). The Late Miocene to Holocene succession thickens basinwards into the axis of the Kangaroo Syncline, and thins to the east and west, towards the NW Shelf and the crest of Exmouth Plateau respectively (Nugraha et al., 2018).

## 3 | DATASET AND METHODOLOGY

In this study, we use two types of seismic reflection data provided by Geoscience Australia (http://www.ga.gov.au/nopims): (a) up to ca. 500 km long, 2D seismic reflection surveys, which were collected between 1993 and 2005; and (b) a 3D seismic reflection survey (Willem 3D seismic survey), which was acquired by Veritas DGC Australia in 2006. The Willem 3D seismic survey covers a total area of ca. 2,628 km$^2$, extending along the Exmouth continental slope and across the lower slope into the Kangaroo Syncline (Figure 2a,b). A downward decrease and increase in acoustic impedance are expressed as blue (negative) and red (positive) reflection events, respectively (Figure 3a). We estimate the vertical resolution of the Willem seismic survey using the frequency content (ca. 60 Hz decreasing to ca. 40 Hz) and average seismic velocity (1,500 m/s decreasing to 2,000 m/s)

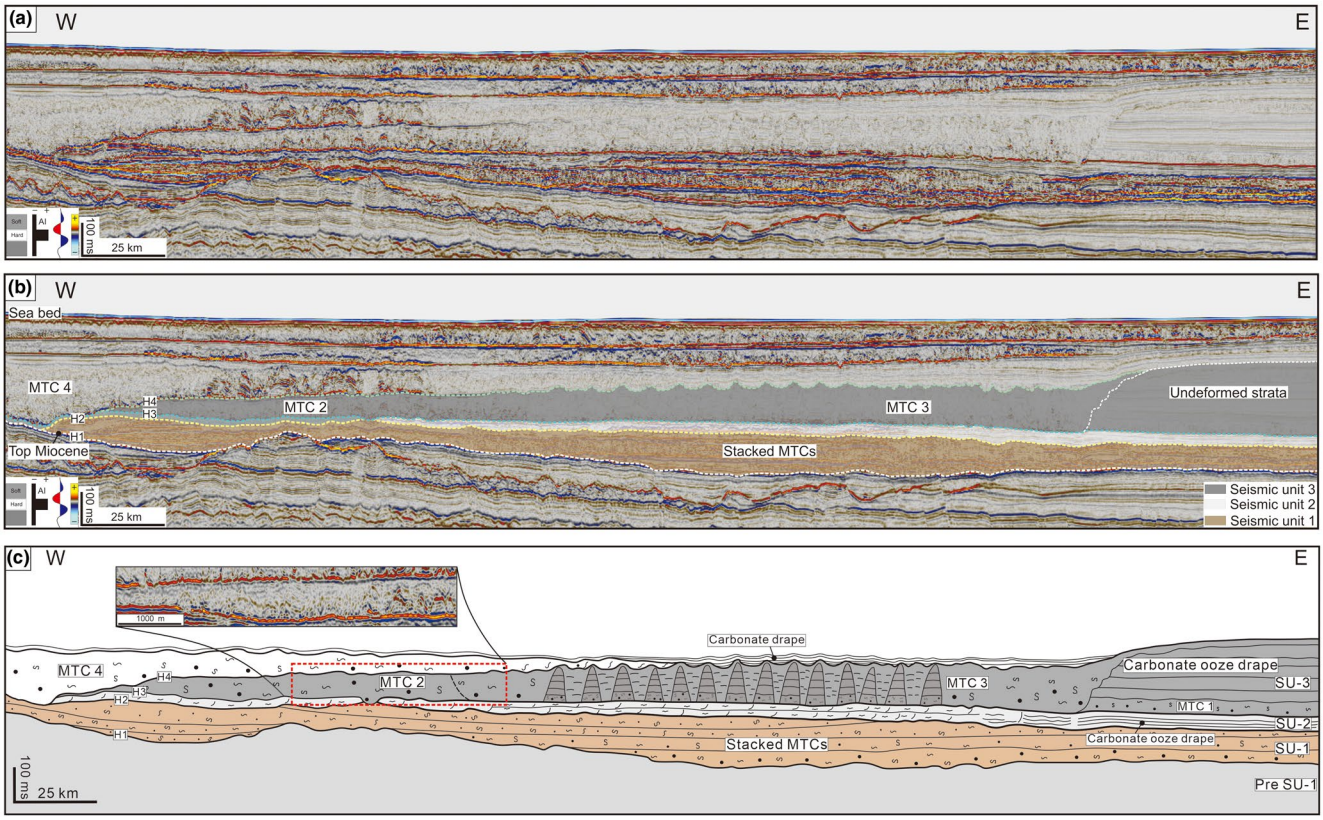


**FIGURE 3** (a) Un-interpreted regional seismic section; (b) Interpreted regional seismic section highlighting the key horizons and the seismic units the study area, note that the horizon H1 is the same horizon of Horizon C (see detail from Nugraha et al., 2018) which defines an unconformity of late Miocene (ca. 9 Ma); (c) Interpretation sketch of the regional seismic section. See Figure 2b for location

between the seafloor and H1. Based on these data, we calculate an approximate vertical resolution of 6.25 m at the seafloor, decreasing to 11 m near the base of the studied interval. This imaging quality is sufficient to map, at relatively high resolution, the geometry of structural features (e.g. scours, faults, etc) immediately below and within the studied MTC.

We adopt the seismic-stratigraphic framework of Nugraha et al. (2018), which is based on their analysis of the Exmouth Plateau, ca. 50 km SW of the study area (Figure 2a). Our study interval falls within SU3 of Nugraha et al. (2018), within which we mapped four key horizons (H1-H4; Figure 3b) in this study based on their strong amplitude, continuity (i.e. they are regionally mappable and extend across the study area) and stratigraphic distribution (i.e. they are relatively evenly distributed throughout the stratigraphic succession of interest). Horizon H1 (Figure 3b) is a regionally mappable unconformity that defines the base of the Upper Miocene and which formed as the result of the collision of the Australian and Eurasian plates (Boyd et al., 1993; Hull & Griffiths, 2002). The lithology and geotechnical properties (i.e. water content, porosity, shear strength, etc.) of the studied stratigraphic interval are inferred from ODP Sites 762 and 763, which are located ca. 300 km SW of the study area where they penetrate a similar seismic-stratigraphic succession.

We extracted seismic attributes, such as variance and amplitude contrast (see Appendix S1 for explanation), from the 3D seismic reflection dataset to determine the external geometries and geomorphology of the imaged deep-marine deposits (Brown, 2011; Chopra & Marfurt, 2007). The dimensions of the MTC-hosted blocks have been quantitatively analysed based on their morphological characteristics: (a) *block height*, which is the height between the crest and base of the blocks (i.e. the MTC basal shear surface; Figure 6b); (b) *block spacing*, which is the spacing between the mid-point of the crests of two adjacent blocks (Figure 6b); (c) *block tip angle*, which is the angle between the block tip and vertical (Figure 6b); and (d) *block friction angle*, which is the angle between the side of the blocks relative to their base surface (Figure 6b).

## 4 | SEISMIC-STRATIGRAPHIC ANALYSIS

### 4.1 | SU-1 and SU-2

We divided the studied stratigraphic interval into three seismic units (SU-1-3; Figure 3b,c). SU-1 is ca. 500 m thick

near the axis of the Kangaroo syncline, thinning westward and eastward to ca. 200 m. SU-1 contains packages of chaotic, medium- to high-amplitude seismic reflections interpreted as stacked MTCs (Figure 3b,c) (Hengesh et al., 2012; Nugraha et al., 2018). SU-2 is thinner than SU-1, but also varies in thickness, being slightly thicker near the centre of the Kangaroo Syncline (c. 60 m) and thinning gradually westward and eastward to ca. 30 m (Figure 3b). SU-2 contains two distinct seismic facies: (a) continuous, low- to medium-amplitude, sub-parallel seismic reflections in the east; and (b) discontinuous to chaotic seismic facies in the centre and west (Figure 3b,c). The continuous seismic facies is interpreted as slope-to-basin floor, carbonate ooze deposits, whereas the more discontinuous seismic facies is interpreted as deformed carbonate ooze drape deposits (Nugraha et al., 2018). Variance attribute-based analysis of the base of SU-2 (Horizon H2) in the central part of the study area reveals a concentrated high variance response with circular shape in an NW-SE linear trend (Figure 5a). These high variance circles form bulges in seismic section that are ca. 30–70 m in diameter, disaggregating the overlying strata (see the seismic section in Figure 5a). Based on their size, geometry and distribution, these circular bulges are interpreted as fluid expulsion-related pockmarks (e.g. Plaza-Faverola et al., 2011). Fluid escape features such as these are common on the Exmouth Plateau (i.e. Velayatham et al., 2018, 2019).

## 4.2 | SU-3

SU-3 is ca. 500 m thick in the axis of the Kangaroo Syncline, gradually thinning westwards due to truncation below MTC 3 (Figure 4a,b). We identified three distinct seismic facies in SU-3, which we describe below (pre-MTC 3, MTC 3 and MTC 2; Figure 3b).

### 4.2.1 | Pre-MTC 3

The pre-existing interval defines the eastern part of SU-3 and is characterised by a thin (70 ms TWT; 25% of the total thickness of SU-3) package of chaotic to discontinuous, low- to medium- amplitude seismic reflections at its base, which is overlain by a thick (170 ms TWT; 75% of the total thickness of SU-3) package of continuous-to-locally slightly wavy, low- to medium-amplitude seismic reflections (Figure 3c). The chaotic seismic facies is interpreted as an MTC (MTC 1), whereas the continuous seismic facies likely represents carbonate ooze (Figure 3b,c; Nugraha et al., 2018).

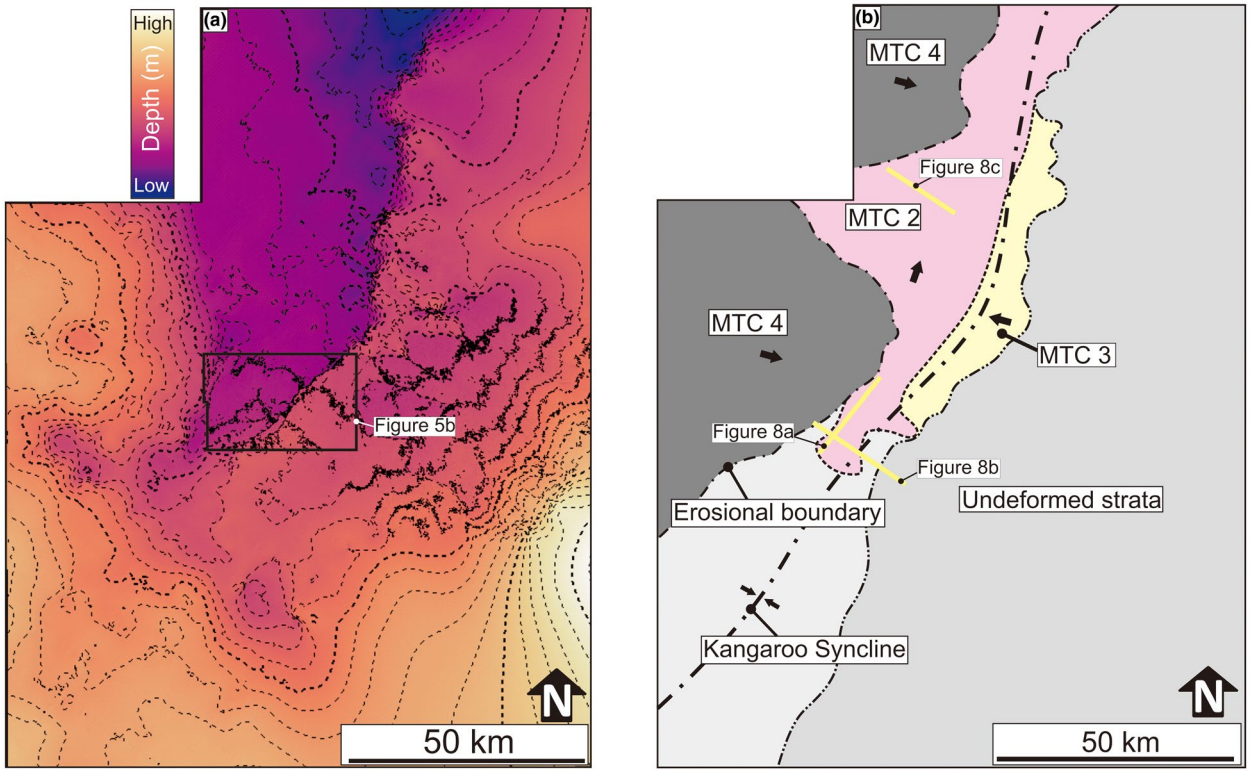


**FIGURE 4** (a) Regional structure map interpreted based on the 2D and 3D seismic reflection data, showing the depth structure calculated on horizon H3; (b) sketch of the regional structure map showing the distribution of the key intervals in SU-3 (undeformed strata, MTC 3, and MTC 2)

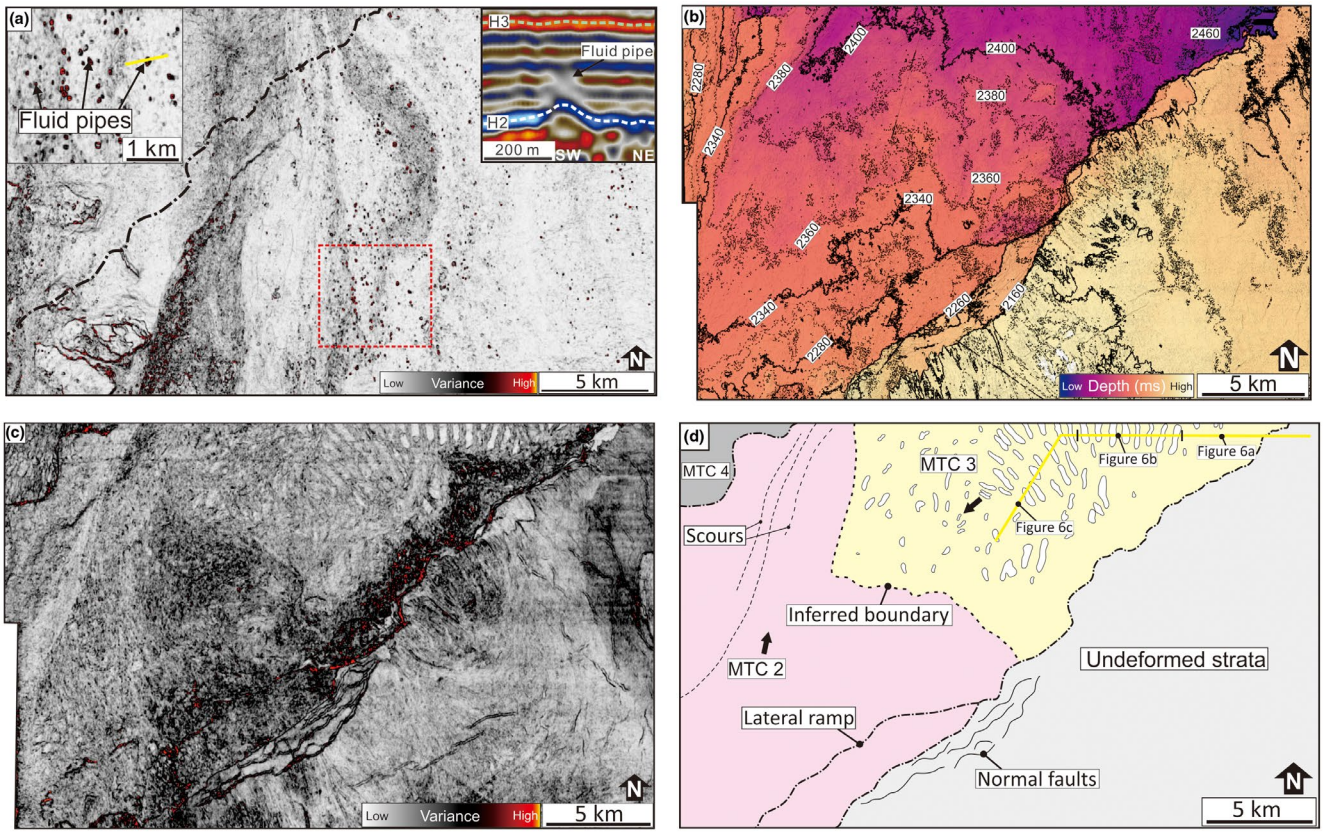


**FIGURE 5** (a) Variance attribute calculated on Horizon H2 within the 3D seismic reflection data area, revealing pipe-like structures. The dashed line indicates the same boundary in (d) between the undeformed and deformed strata. The upper left map shows the zoom-in view of pipe-like structures, and the upper right seismic section shows the seismic cross-section of the fluid pipe; (b) depth structure map calculated on basal shear surface of the MTC 3 within the 3D seismic area; (c) variance attribute calculated on Horizon H3 within 3D seismic area; (d) sketch of the MTC 3 deposit, revealing the key intervals in SU-3 (undeformed strata, spread, and MTCs)

## 5 | SEISMIC CHARACTERISATION OF MTCS

We identify four post-Early Miocene MTCs (MTC 1–4; Figure 3b,c) in SU-3. We describe these MTCs from east to west, following the naming convention of MTC 3 (i.e. most easterly), 2 (i.e. central) and 4 (i.e. most westerly).

### 5.1 | MTC 3

#### 5.1.1 | Description

MTC 3 defines the central part of SU-3, near the axis of the Kangaroo Syncline, where the seafloor presently dips very gently (c. 0.4°) (Figure 4b). Approximately 1,050 km$^2$ of MTC 3 is imaged in the 3D seismic data, although 2D seismic data show the deposit covers ca. 3,600 km$^2$ (Figures 4a,b and 5b-d). We describe MTC 3 with respect to the following features: (a) the geometry of its basal shear surface and seismic facies of its substrate, (b) the seismic facies and geometrical characteristics of its contained blocks and troughs and (c) its overall geometry and the geometry of its top surface.

**(i)** The basal surface of MTC 3 is characterised by a continuous, high-amplitude, positive seismic reflection (Figure 6a). In the east, this surface merges with the basal shear surface of MTC 1 (Figure 6a). The basal surface of MTC 3 does not contain any seismic-scale erosional features such as scours, striations or grooves (Figure 5c,d) (e.g. Bull et al., 2009a; Sobiesiak et al., 2018). As such, it is not easy to determine the MTC transport direction. However, the surface defines a sharp boundary between different facies (i.e. weakly deformed below and very chaotic above), and the high-amplitude character supports an interpretation of a basal shear surface (e.g. Wu et al., 2019). The 60 ms TWT thick (ca. 60 m) unit immediately underlying and representing the substrate of MTC 3 ranges from discontinuous and moderately deformed near the eastern-margin of MTC 3, to chaotic and highly deformed near the proximal part of the deposit (Figure 6a,b).

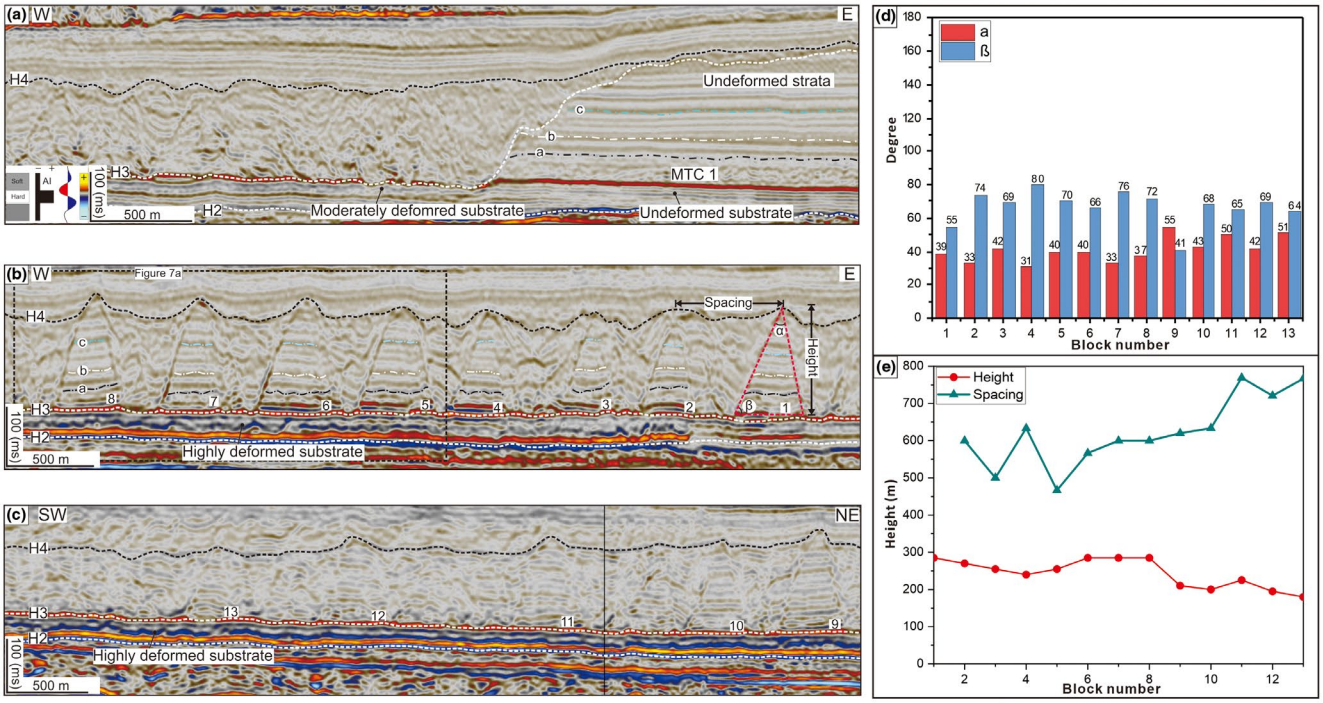


**FIGURE 6** (a) Seismic section showing the eastern boundary of the MTC 3 and the undeformed strata; (b) seismic section showing the proximal section of the MTC 3; (c) seismic section showing the distal section of the MTC 3. See the location from Figure 5d; (d) the calculation of the tip angle (α) of the blocks and the friction angle of the blocks to the failure surface (β); (e) the calculation of height and the spacing of the blocks. See block number from (b and c), and the block number refers to the order in which the blocks are away from the undeformed strata

**(ii)** Map-view images show that MTC 3 contains parallel to sub-parallel, block-shaped packages (Figure 5c,d). In seismic cross sections, these form ridge-shaped blocks flanked by troughs (Figure 6b). The blocks are 210–300 m high, 170–210 m wide and 800–1,200 m long are relatively undeformed (Figure 6b). The intervening troughs are 160–260 m high, 190–230 m wide, 800–1,200 m long and are defined by a very chaotic, variable-amplitude seismic facies.

All the blocks contain two distinct seismic facies that are similar to those defining undeformed slope strata outside of the MTC (Figure 6a,b). Seismic reflection within the blocks are sub-horizontal and are approximately parallel to the basal shear surface and underlying substrate strata. Three seismic reflections, intra-block reflections a-c, are identified within the blocks, which can be correlated with confidence from block-to-block over a large area (seismic reflection a-c; Figure 6b). However, the blocks become more disaggregated, and their external form become less pronounced, adjacent to the headwall in the E and adjacent to its toe in the SW. Downslope, intra-block reflections a-c become harder to identify and trace (Figure 6c). The blocks ultimately become extremely chaotic in the distal part of MTC 3, showing similar facies to MTC 1 (Figure 6c). Upslope, the relationship between the blocks and the undeformed strata shows a clear increasing deformation systematically eastward (Figure 6a). The average tip angle of the blocks is ca. 38°, with little variability about this value (Figure 6d). The angle of the tip to the basal shear surface ranges from 55 to 80° (average 71°) (Figure 6d). The height of the blocks gradually decreases downslope to the SW towards the distal end of MTC 3, from ca. 290 m to ca. 190 m (Figure 6e). Block spacing increases towards the SW, from ca. 610 m near the centre to ca. 760 m near the distal region of MTC 3 (Figure 6e).

The intra-block troughs are characterised by moderately discontinuous to chaotic seismic facies (Figure 6b). By blending variance and amplitude data we see that the troughs contain numerous ‘v’-shaped, vertical to sub-vertical, pipe-liked structures that extend from the basal shear surface of MTC 3 to its top. We refer to these ca. 280 m tall, up to 100 m diameter features as ‘subvertical deformation zones’ (SDZs) (Figure 7a). Within troughs, seismic reflections are mostly sub-horizontal and discontinuous, the edge of the reflections can be as steep as 50° near the trough margin (Figure 7a). Locally, where the magnitude of intra-trough deformation is low, we can trace seismic reflections from within the troughs into adjacent blocks (see the coloured dots in Figure 7a). The width of the SDZs increase upward, from ca. 40 m at their narrowest basal point to up a few hundreds of metres at their tops (Figure 7b and c).

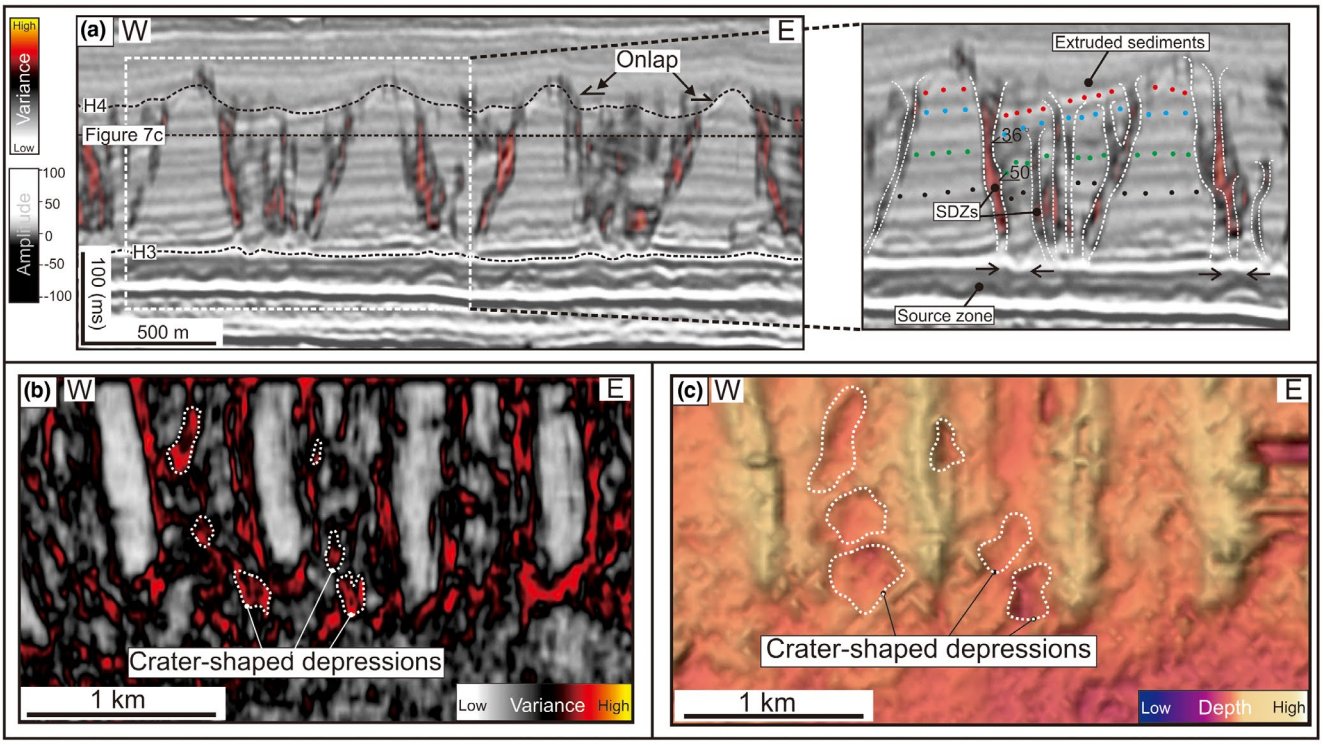


**FIGURE 7** (a) Seismic characteristics of pipe structures in the seismic section with an overlay of the variance attribute (left), and a zoomed-in view of the SDZs (right), showing the details of the pipe-like fluid escape structures, see the location in Figure 6b; (b) variance time slice through the troughs, showing the crater shaped pipes. See the time slice location in (a); (c) structure map of the horizon H3, showing the top structure of the blocks in MTC 3; see the location of the structure map in (a). Please also note that the diameters of the crater-shaped depressions increase upward, from ca. 80 m in the variance time slice to hundreds of metres in the structure map

**(iii)** The top of MTC 3 is characterised as a rugose low-amplitude, positive seismic reflection. The crests of intra-MTC blocks define locally positive relief that are onlapped by overlying reflections, whereas intervening troughs define concave-up structural lows (Figure 6a,b). The SDZs extends throughout the vertical extent of the trough, and reflections onlap the blocks (Figure 7a).

### 5.1.2 | Interpretation

The similarity in the seismic facies succession characterising the intra-MTC blocks and the undeformed strata (i.e. a thin MTC overlain by largely undeformed, slope-to-basinfloor strata) suggests the former are derived from the latter. This is supported by the blocks in the eastern part of MTC 3 being the same thickness as the laterally adjacent, largely undeformed interval. We therefore interpret the boundary between MTC 3 and the undeformed strata is the MTC headwall. The fact we can correlate the intra-MTC seismic horizons (reflection a-c; Figure 6a,b) within the blocks and flanking, more highly deformed troughs, suggest that the blocks were initially transported as a coherent mass. The continuity of the intra-block reflections also indicate that the blocks were only weakly deformed during the transport.

We interpret that the westward decrease in block height and spacing, normal to the broadly NE-trending headwall, suggests that MTC 3 was translated westwards, approximately perpendicular to the depth contour of the interpreted base of the MTC 3 (Figure 5b,d). We also note that the amount of deformation below MTC 3, inferred from the thickness of the highly deformed package, increases westwards at the transition from beneath the relatively thin MTC 1, which forms part of the pre-existing, broadly undeformed slope strata, to below the relatively thick MTC 3. The low degree of internal deformation, limited distance from the headwall and lack of kinematic indicators supports an interpretation that the blocks moved a limited horizontal distance. Therefore, we suspect that the relatively highly deformed nature of the substrate near the proximal part of MTC 3 may not have been directly caused by shearing of the substrate by the overlying mass. We instead interpret that this deformation occurred due to the presence and catastrophic failure of an overpressured substrate by liquefaction or strain softening, which both would have caused intense stratal disruption. Similar liquefaction-driven seismic

facies (i.e. medium- to high-amplitude, chaotic seismic reflections) are described in the literature (e.g. Ogata et al., 2014).

The moderately deformed reflections defining the SDZs indicate modest internal deformation within these areas. We infer that the SDZs represent vertical fluid migration conduits, which drove fluid expulsion from the underlying, over-pressured substrate (e.g. Cartwright & Santamarina, 2015; Løseth et al., 2011; Moss & Cartwright, 2010). The overlying elliptical depressions, which define structural lows along the top of MTC 3, reflect overburden collapse due to the expulsion, upward migration and expulsion of deeper material. Seismic reflections onlapping blocks protruding from the top surface of MTC 3 may represent the extruded sediments or subsequently deposited deep-water sediment (e.g. Clari et al., 2004; Roberts et al., 2010; Watkinson & Hall, 2019).

### 5.2 | MTC 2

MTC 2 occurs in the western part of SU-3 (Figures 4b and 5c,d). This deposit is deeply eroded on its NW margin by a subsequent mass failure event (MTC 4), and is hard to differentiate from MTC 3 in the NE (Figures 4b and 5d). However, the boundary between MTC 2 and 3 can be inferred from their slightly differing seismic facies; MTC 3 is defined by an overally higher amplitude, blockier seismic facies, whereas MTC 2 is defined by overall lower amplitude, chaotic seismic facies (Figure 3a-c). MTC 2 has an NW-trending headwall (Figure 8a) and NE-SW trending lateral margins (Figure 8b), and comprises low- to very low-amplitude, chaotic reflections. In the northern part of the Kangaroo syncline, MTC 2 increases in thickness away from its headwall, from ca. 70 ms near its headwall (Figure 8a) to ca. 200 ms further NE (Figure 8c). The orientation of the headwall scarp and lateral margins suggest that MTC 3 was transported towards the NNE, following the overall dip of the Kangaroo Syncline (Figure 4b).

### 5.3 | Stratigraphic evolution

Based on the observations made above, we propose that the study area has experienced several episodes of slope failure-driven erosion and deposition (Figure 9). First, multiple, stacked MTCs were deposited (SU1; Figure 9a) that were subsequently draped by carbonate ooze (SU-2; Figure 9b). Gas or fluids, sourced from deeper stratigraphic levels, migrated upward into SU-2 (Figure 9b). During the initial stage of SU-3 deposition, an MTC was emplaced (MTC 1), which was overlain by a thick, carbonate ooze-bearing sequence (Figure 9c). MTC 2 was subsequently emplaced in the west of the study area (Figure 9d). The removal of sediment during the evacuation of MTC 2 likely had a debuttressing effect, promoting subsequent slope failure and the triggering of MTC 3 through removal of lateral and down-slope confining support (Figure 9d). As a result of overpressure released by slope failure, sediments extruded from below MTC 3 were transported upward through, and deposited on top of, the overlying mass. MTC 4 was subsequently emplaced in the west of the study area on top of MTC 3, followed by draping of the entire succession by carbonate ooze (Figure 9e).

## 6 | DISCUSSION

### 6.1 | Was MTC 3 emplaced by creep- or spread-related processes?

Creep is a gravity-driven process, with the updip margins defined by retrogressively formed faults and folds (Lee & Chough, 2001; Li et al., 2016). In contrast, spreading occurs above a precursor failure surface, with the failed mass translating laterally and being broken into blocks and troughs that are bounded by internally generated faults (Micallef et al., 2007). Subaqueous creep has been reported from relatively steep slopes (>3°) (i.e. Shillington et al., 2012; Silva & Booth, 1984), whereas subaqueous spread is reported from gentler slopes occur (<1°) (i.e. Micallef et al., 2007). Although we have not undertaken a balanced structural restoration to investigate the slope dip at the time of MTC 3 emplacement, it is likely that, given its current position beneath the present basin floor, some ca. 300 km from the Late Miocene shelf margin, it was deposited on a gently dipping slope (<1°). The coherent blocks within MTC 3 occur above a low-angle failure surface, suggesting that gravity played only a minor role in their formation, as well as that of the MTC in which they are contained. The blocks are also bound by numerous sub-parallel faults that are of very similar dip; such features are strongly characteristic of the deposits of spreads, rather than creep (Micallef et al., 2007).

Similar block-like features are observed in seismic reflection data in the Ursa Basin, Gulf of Mexico (Sawyer et al., 2009; Sawyer & Hodelka, 2016), and along the Norwegian continental margin (Baeten et al., 2013, 2014; Bryn et al., 2005; Bull et al., 2009b; Micallef et al., 2007), the Hikurangi Margin of New Zealand (Couvin et al., 2020; Micallef et al., 2016) and the Northwest African continental margin (Li et al., 2017). In most cases the blocks are located close to the MTCs upslope margin (i.e. headwall area); where elongate, their long axes are oriented parallel to sub-parallel to the headwall scarp (e.g. Baeten et al., 2013; Li et al., 2017; Micallef et al., 2007). The blocks are cone-shaped, with rounded or semi-rounded crests. The blocks are internally coherent, and are separated by moderately deformed troughs (e.g. Bull et al., 2009b; Couvin et al., 2020; Sawyer

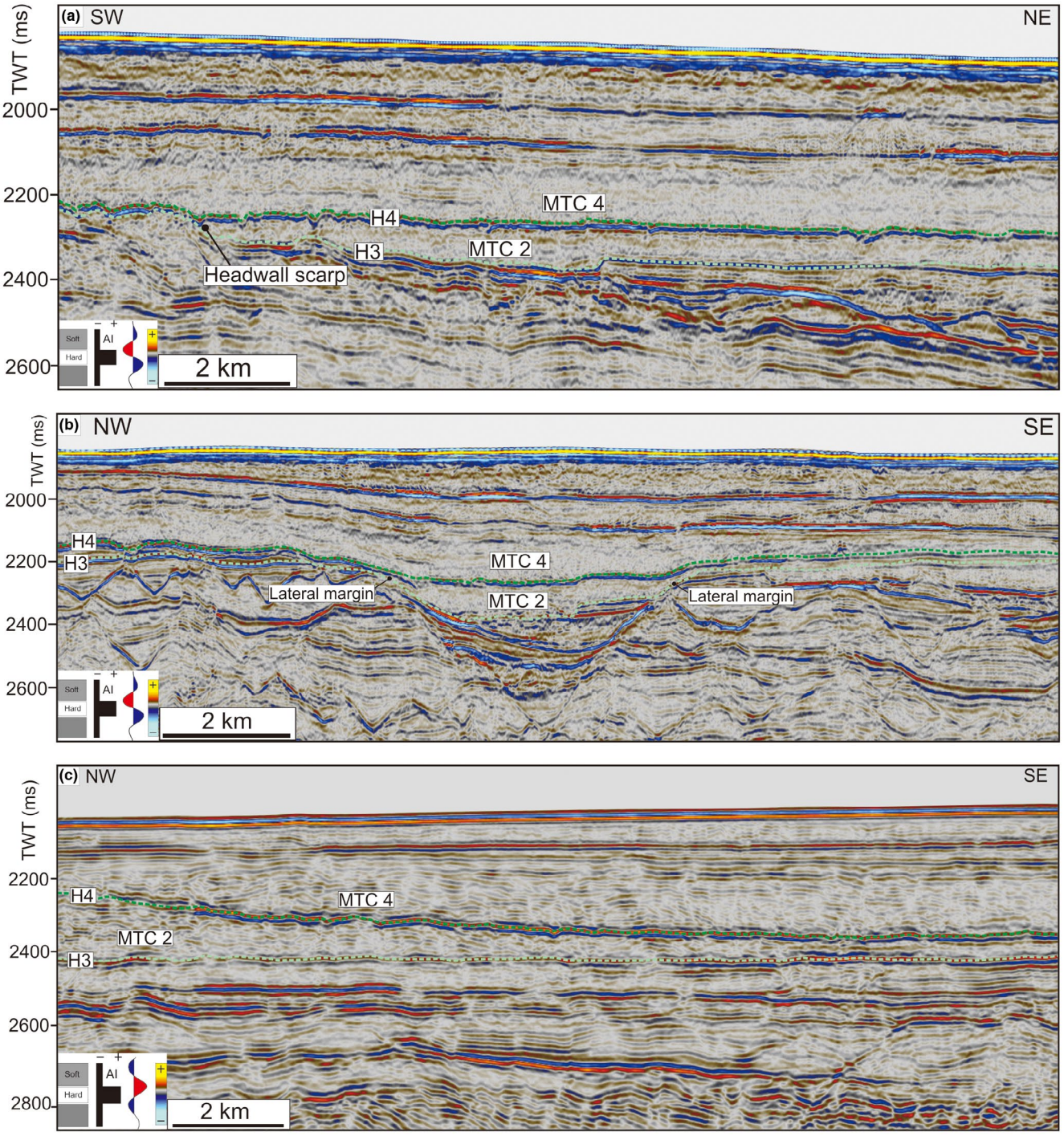


**FIGURE 8** (a) Seismic cross-section through the headwall scarp area of MTC 2; (b) seismic cross-section through the lateral margins of MTC 2; (c) seismic cross-section through the body of MTC 2

et al., 2009; Sawyer & Hodelka, 2016). The blocks are typically smaller than those encountered in our study, being ca. 15–40 m tall (Baeten et al., 2013; Couvin et al., 2020). Block size typically decreases towards downslope, whereas block spacing and internal deformation increases (e.g. Baeten et al., 2013; Li et al., 2017). Based on their geometric characteristics and distribution these blocks are also interpreted as being related to lateral spreads.

The deformed troughs from offshore Norway have been interpreted as being the result of fracturing of the adjacent blocks (Baeten et al., 2013; Laberg & Vorren, 2000), or as the depositional product of debris flows originating from a separate failure event (Couvin et al., 2020). Most of the troughs from published examples have no pipes structures observed within or below the troughs, with exception of examples presented by Huvenne et al. (2002) from the SW Ireland, and

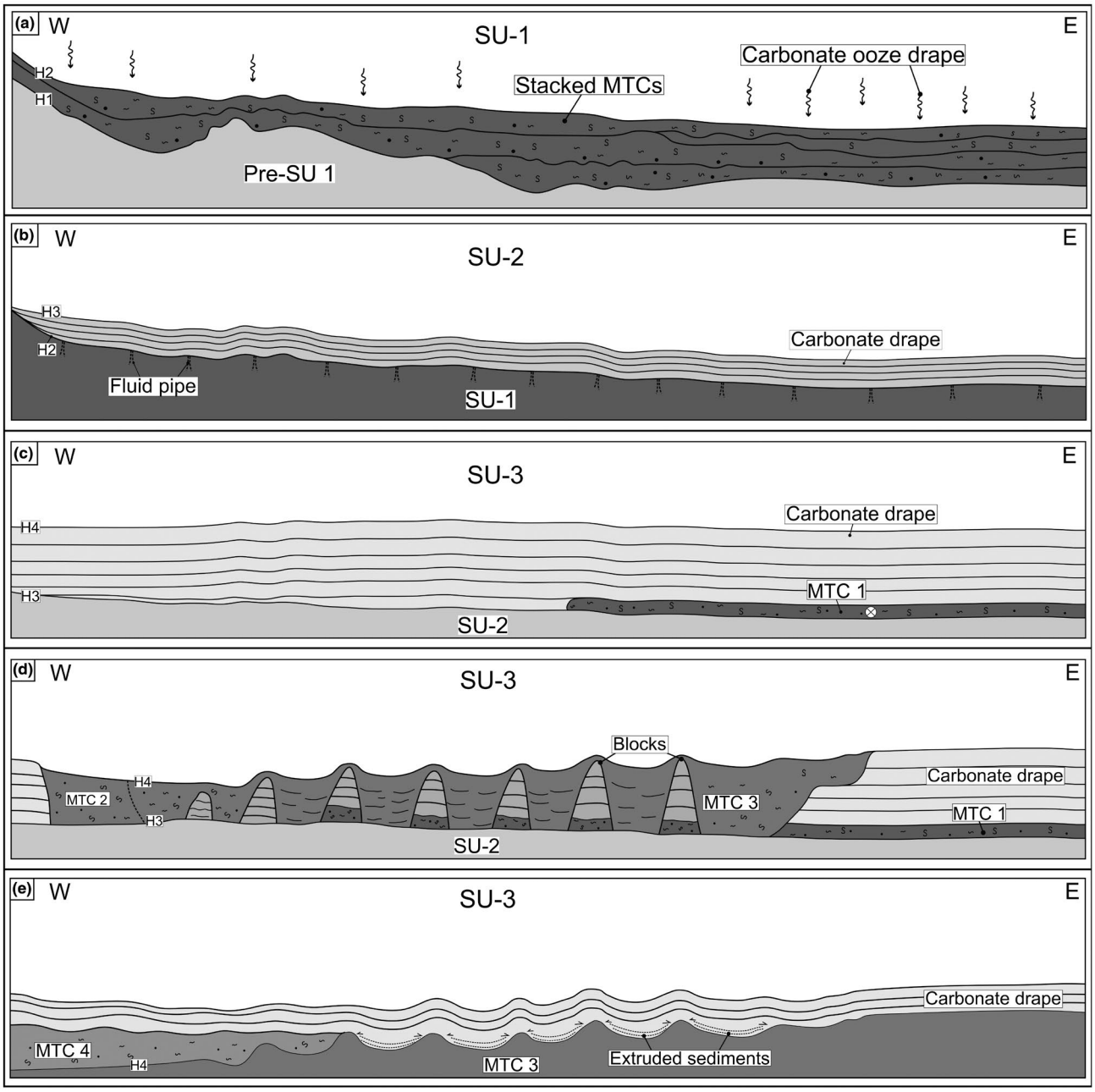


**FIGURE 9** Stratigraphic evolution of the study area. (a) Seismic unit 1 (SU-1), mainly comprises chaotic seismic reflections and deposited as MTCs; (b) seismic unit 2 (SU-2), mainly consists of well-layered seismic section and deposited as carbonate drapes; (c) the initial stage of seismic unit 3 (SU-3), consists MTC 1 and carbonate drapes; (d) the following stage of SU-3, consisting coherent blocks and chaotic intervening troughs; (e) the final stage of SU-3, mainly consists erupted sediments followed by carbonate drapes

by Scarselli et al. (2019) from the NW Shelf of Australia. Fluid pipes may be truly absent, or they may be present but simply not imaged in seismic reflection data. However, pockmarks, which could be linked to fluid escape pipes, are observed near the headwall of Storegga Slide, offshore Norway (e.g. Hustoft et al., 2010; Micallef et al., 2009), as well as the updip margin of the Tuaheni Slide, offshore New Zealand (Carey et al., 2019; Micallef et al., 2016).

Similar blocks have also been observed from exposures in eastern Canada, Scandinavia, eastern southern Italy, SE Crete, Ireland and Indonesia (e.g. Alves, 2015; Dykes & Warburton, 2007; Fortin et al., 2008; Hungr et al., 2014; Jablonská et al., 2018; Locat et al., 2011, 2017; Odenstad, 1952; Watkinson & Hall, 2019). Water ponding and sand injections are observed within the troughs adjacent to the blocks in some of these onshore analogues (Dykes & Warburton, 2007; Locat et al., 2011, 2017; Watkinson & Hall, 2019). When taken together, observations from buried and exposed examples indicate that the fluid escape may play a key role in the formation of giant blocks in submarine spreads.

## 6.2 | MTC 3 emplacement model

### 6.2.1 | Stage 1: Priming

Before the emplacement of MTC 3, the basal shear surface of MTC 1 may have represented a hydraulic boundary between the overlying ca. 300 m thick sediment pile, and the underlying substrate, defined by sharp decrease in permeability and density (i.e. Madhusudhan et al., 2017; Wu et al., 2019) (Figure 10a,b). Excess pore pressure could have built up at this boundary, driven by the ascent of fluids from the lower SU-2 and SU-1 (Figure 10a,b). The properties of the biogenic carbonate ooze sediments (i.e. low permeability, high water content, fine-grained) defining the substrate of the eventual spread may have a direct contribution to the build-up of pore pressure (Bryn et al., 2005; Bull et al., 2009b; Kvalstad et al., 2005; Urlaub et al., 2015). There is also ample evidence that during the early Miocene to Pliocene, the Exmouth Platform was seismically active, with the Kangaroo Syncline representing an inversion-related structure linked to the collision of the Indo-Australian and Eurasian plates (Keep et al., 2007). Related seismicity may have reduced the shear strength of sediments, and built up the pore fluid pressure within the substrate of MTC 3. The increased pore pressure was transferred laterally westwards away from, and sealed by, the overlying basal shear surface of MTC 1 (Figure 10a) (see also examples of pore pressure lateral propagation from Aylsworth & Lawrence, 2003; Legget & LaSalle, 1978).

### 6.2.2 | Stage 2: Distal evacuation

We suggest that MTC 3 was triggered due to the removal of material from its distal margin by the emplacement of MTC 2. The absence of a buttress after northward transport would have removed the lateral confining pressure within the western part of the pre-spread strata to drive the spreading (Figure 10c). The sediments immediately around the debuttressing became a flow (i.e. slump), due to the biogenic structure of carbonate ooze that is rapidly destroyed under loading, transitioning from a coherent to fully disaggregated chaotic mass in a relatively short distance (i.e. 10–20 km; Principaud et al., 2015; Watson et al., 2019). Slope failure caused by the lateral removal of material is termed as 'Rankine active failure' (Lambe & Whitman, 1969). Similar mechanisms have also been documented in the Gulf of Mexico (Sawyer et al., 2009), offshore Norway (Baeten et al., 2013; Bull et al., 2009b), offshore New Zealand (Couvin et al., 2020) and offshore Africa (Li et al., 2017). The lateral removal of material and the associated open space could be created by a failure event (e.g. Baeten et al., 2013; Bull et al., 2009c; Li et al., 2017; Micallef et al., 2007; Sawyer et al., 2009). The effect of the lateral removal of material (i.e. debuttressing) is to initiate an extensional strain in the material behind that open space, and ultimately form lateral spreads. However, we speculate that debuttressing and spread initiation could also be achieved by submarine erosion by turbidity currents and/or bottom currents, albeit over a longer period (e.g. Couvin et al., 2020; Locat et al., 2011).

To the east, the sediment pile was primed to fail for the reasons outlined above (i.e. excess pore pressure; Figure 10a). The low gradient (ca. 0.4°) of the basal shear surface of MTC 3 likely prevented the failure from accelerating and translating a great distance during emplacement. As a result, the intra-spread blocks stayed relatively intact compared to failures occurring on more steeply dipping slopes (i.e. Hengesh et al., 2013). Onshore and offshore data indicate that even small amounts of unloading near the down-dip part of the slope can trigger the formation of spreads (i.e. Broussard, 2014; Kvalstad et al., 2005; Locat et al., 2011; Micallef et al., 2007).

### 6.2.3 | Stage 3: MTC 3 initiation

The mass comprising MTC 3 started sliding westward into the new space created by the movement northwards of MTC 2 (Figure 10c). Additional shearing and deformation below MTC 3 ruptured the base-MTC 1 seal layer, promoting liquefaction of the substrate in over-pressured zone, which drove the upward transport of fluids and the formation of large pipe-like structures.

The tip angle ($\alpha$) and the friction angle of the block ($\beta$) follow a relationship of $\beta \approx 90° - (\alpha/2)$, which aligns with the failure surface angles observed from triaxial experimental tests on intact natural clays (Lambe & Whitman, 1969; Locat et al., 2011, 2015). This relationship suggests that internal shear fractures were generated during spreading. Two sets of hydraulic internal shear fractures (primary/secondary internal shear fractures) formed and propagated upwards due to the high fluid over-pressure in the substrate (Figure 10c). The primary internal shear fractures developed a 'V'-shaped geometry, consistent with the predictions of numerical models of sediment failure (Andresen, 2001; Buss et al., 2019; Dey et al., 2016; Kvalstad et al., 2005). In between the primary internal shear fractures, smaller secondary shear fractures propagated upward from the basal shear surface of MTC 3 (e.g. see also the formation process of the hydraulic fracturing related pipes from Cartwright & Santamarina, 2015; Løseth et al., 2011; Sun et al., 2013). The lateral movement of the spread will increase the shear stress in the substrate of MTC 3, driving growth of the primary and secondary fractures. Overlying material was ultimately broken into fracture-bound blocks flanked by troughs.

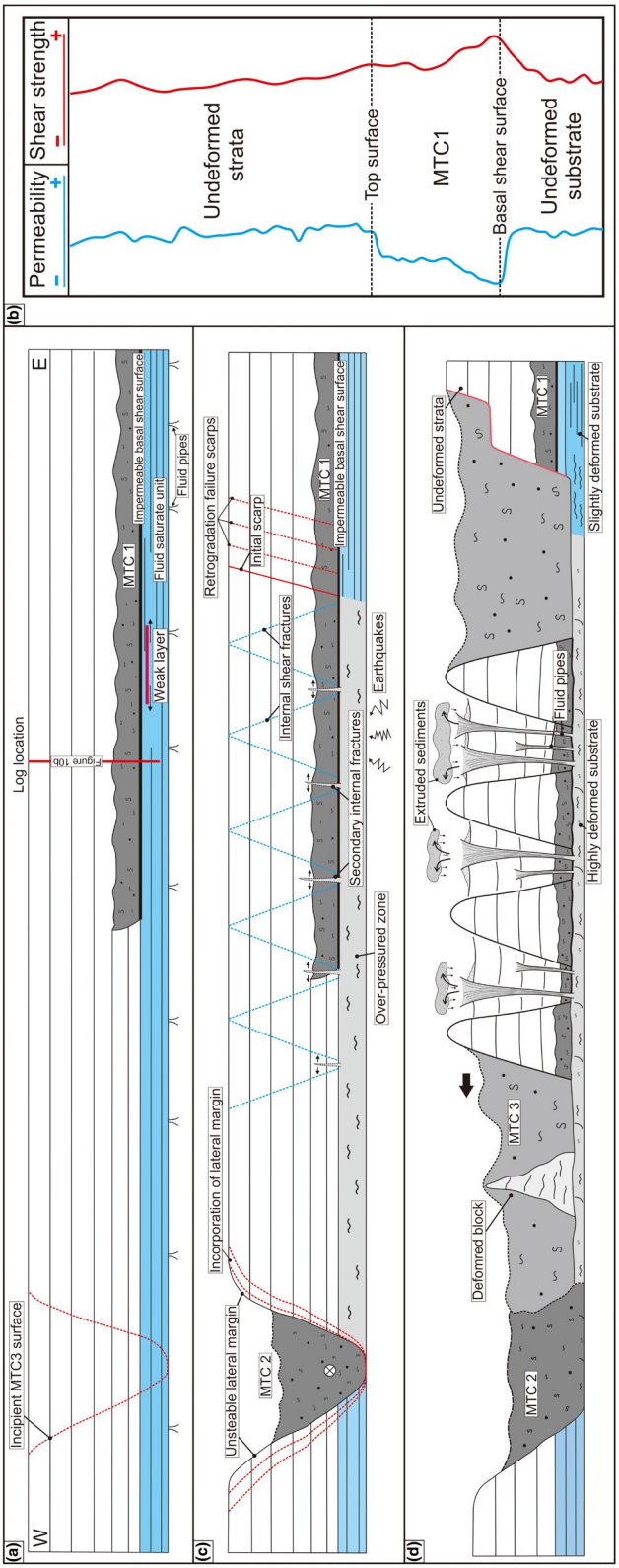


**FIGURE 10** Schematic diagram showing the development of the spread: (a) Deposition of the undeformed sediments, MTC 1 and down dip evacuation of the MTC 3; (b) inferred permeability and shear strength curve through undeformed strata; (c) overpressure induced primary and secondary internal fractures propagation stage; (d) sediments dislocated into blocks and troughs with extruded sediment deposition stage

### 6.2.4 | Stage 4: Internal deformation and lateral spreading

Overpressured substrate fluid-sediment mixes flowed upward via the secondary internal shear fractures within sub-circular fluid pipes (e.g. Cartwright & Santamarina, 2015). This extruded material was deposited in depressions above the troughs on the top surface of MTC 3 (Figure 10d). Blocks near the distal end of MTC 3 underwent a greater lateral displacement and deformation with increase release of the excess pore pressure from the base of the spread compared to proximal areas that moved less far. Due to the release of overpressure, the shear stress required to drive horizontal motion increased, which may ultimately stop spreading. The spreading may also stop because the mass hit the far (eastern) of the existing MTC 2 lateral margin (Figure 10d). There is an increasing deformation near the headwall of the spread. This is because the failed sediments of MTC 3 moved west first, and this might have ended up with a 'hole' in the east near the initial scarp. The initial scarp was later failed retrogressively, leaving a step-like headwall scarp, and a mass of strongly deformed sediments next to the headwall (Figure 10d).

## 6.3 | Implications

### 6.3.1 | Preconditioning and triggering of spreads: Unloading and lubrication

We have investigated the geometry and internal structure of an MTC, inferring it was related to a submarine spread. Our study shows that, in these cases, spreading can occur even if the slope gradient is presently low. We propose that the spread was *primed* by the presence of an overpressured layer, which acts as a basal shear surface and promotes sliding on a very low-angle slope. Slope failure was ultimately *triggered* by debuttressing of the slope mass by an earlier slide, which removed downslope and/or lateral confinement. Together these processes resulted in a short run-out but highly deformed slide mass. While the spread shows abundant evidence for intense internal deformation, we relate this deformation to fluid escape from subsurface overpressured strata beneath the failing mass, rather than to landslide disaggregation under rapid, long-distance transport. We suggest that the slide mass may have only moved a relatively short distance (i.e. only a few hundred metres) and that the amount of strain observed in landslides is therefore not necessarily a direct indication of transport distance.

### 6.3.2 | The importance of rheology and mobility for geohazard assessments

For offshore geohazard assessments, it is important to understand the mobility and rheology of an MTC (Thomas et al., 2010). If the landslide mass of MTC 3 moved only a short distance and at relatively low speed, then the potential for tsunamigenesis will be low, despite the relatively large volume (ca. 360 $km^3$) of the mass. Numerical modelling has shown that very large landslides (volumes of up to 1,000 $km^3$) may not trigger a tsunami if they commence as relatively slow, retrogressive failures (Løvholt et al., 2017).

The nature of seafloor and subsurface deformation associated with submarine landsliding control the impact this processes has on different offshore structures. For instance, a seafloor-laid pipeline or cable may be able to withstand slow-moving seafloor displacement during a spread, instead being much more vulnerable to the impact of faster moving slides that become frontally emergent and disaggregate to form more mobile debris flows (Lacroix et al., 2020; Thomas et al., 2010; Zakeri, 2009). Piles or top-hole conductors that support platforms or deep-sea field developments may penetrate tens or hundreds of metres below the seafloor. These deeper foundations are susceptible to i) lateral and vertical movements, which may be relatively limited within intact blocks due to the limited transport distance of the MTC; and ii) changes in subsurface pore pressure and the remoulding of sediments, which together may reduce their lateral capacity (i.e. weakening their support); this particularly property may be prognosed by when an intra-block, fluid vertical fluid venting system is identified (Amaratunga & Grozic, 2009; Hong et al., 2017).

### 6.3.3 | Submarine spreads: Underappreciated agents for seafloor fluid flow

Many studies propose fluid migration at depth as a potential preconditioning or triggering factor for MTCs (e.g. Bünz et al., 2005; Deville et al., 2020; Elger et al., 2018); however, few studies link MTCs to syn- or post-emplacement release of fluids (e.g. Bøe et al., 2012; Browne et al., 2020; Yang et al., 2013). It is suggested that significant volumes of methane (an important greenhouse gas) may have been emitted during the disaggregation of the 3,000 $km^3$ Storegga Slide (Paull et al., 2007), and that methane release by widespread submarine landslide activity may have been a contributory mechanism for elevated methane emissions that catalysed the Palaeocene-Eocene Thermal maximum (Higgins and Schrag, 2006). The role of submarine landslides in the release of previously sequestered fluids such as methane remains poorly constrained, and is thus omitted from existing global budgets. Our study shows that fluid escape can play an important role during MTC emplacement, as vertical escape structures act as efficient conduits for fluids and sediments from depth to the seafloor. Similar seafloor fluid expulsions, including that linked to post–MTC emplacement, create cold seeps that support high biomass communities of microbes and

chemosynthetic fauna, as the focused fluid flow creates cold seeps (e.g. Deville et al., 2020). Therefore, as well as disturbing the seafloor, MTCs may also provide important hotspots for deep-sea biodiversity, particularly where they create focused zones of fluid flow.

## 7 | CONCLUSION

We use 2D and 3D seismic reflection data to investigate processes of submarine spreading, on the Exmouth Plateau, offshore NW Australia. The spread comprises: (a) giant, upward-tapering blocks (ca. 300 m-high, ca. 1,200 m-long and ca. 210 m-wide) which are undeformed, and (b) intervening troughs (ca. 260 m depressions separating the blocks), which are moderately deformed. We interpret that the blocks were only transported minimal lateral distance, and the relatively deformed troughs are formed by the expulsion of fluid and sediment during hydraulic failure of the sediment mass. We then developed a new internal hydraulic fracturing model that accounts for the styles and patterns of blocks and the intervening troughs. The new model requires a low gradient prerequisite over-pressured failure surface/zone, the low gradient of the basal shear surface likely prevented the block from accelerating and translating a great distance during emplacement. The new model suggests that the spread is initiated by the removal of materials in the toe of the otherwise stable strata (i.e. debuttressing). The debuttressing of the adjacent strata results in the decrease of the lateral confining pressure within the pre-spread strata, and subsequently, triggers the spreading process. The underlying overpressured layer is important to prime the spreading and explain the scale and style of fluid escape. An improved understanding of the initiation, emplacement and deposition of submarine spreading failures adds to our broader understanding of deep-water mass failure processes, the risks posed to seafloor infrastructure, and the often-complex interactions with local benthic ecology.

## ACKNOWLEDGEMENTS

We would like to thank Geoscience Australia for providing the 2D and 3D seismic reflection data that was used in this study, and Schlumberger are thanked for providing Petrel to Imperial College. We thank the editor, Atle Rotevatn, who handled our manuscript, and reviewers Derek Sawyer and Qiliang Sun for their thoughtful and constructive reviews. We also thank Joe Cartwright and Rebecca Bell for helpful discussions and supportive suggestions. The first author thanks the China Scholarship Council and iRock Technology for its financial support. The fifth author acknowledges funding from the Natural Environment Research Council CLASS National Capability Programme (NE/R015953/1). The seventh author thanks for funding from Guangdong Basic and Applied Basic Research Foundation (2020B1515020016).

## PEER REVIEW

The peer review history for this article is available at https://publons.com/publon/10.1111/bre.12532.

## DATA AVAILABILITY STATEMENT

The data that support the findings of this study are available from the corresponding author upon reasonable request.

## ORCID

*Nan Wu* https://orcid.org/0000-0003-3967-9877
*Christopher A.-L. Jackson* https://orcid.org/0000-0002-8592-9032
*Harya D. Nugraha* https://orcid.org/0000-0001-6099-7947
*Wei Li* https://orcid.org/0000-0002-8260-2042

## REFERENCES

Alves, T. M. (2015). Submarine slide blocks and associated soft-sediment deformation in deep-water basins: A review. *Marine and Petroleum Geology*, *67*, 262–285. https://doi.org/10.1016/j.marpetgeo.2015.05.010

Amaratunga, A., & Grozic, J. (2009). On the undrained unloading behaviour of gassy sands. *Canadian Geotechnical Journal*, *46*(11), 1267–1276. https://doi.org/10.1139/T09-056

Andresen, L. (2001). Effect of strain softening on stability analyses. Analysis of retrogressive sliding due to strain softening—Ormen Lange case study. NGI report(521001–10).

Aylsworth, J., & Lawrence, D. (2003). Earthquake-induced landsliding east of Ottawa; a contribution to the Ottawa Valley Landslide Project, Geohazards 2003, 3rd Canadian Conference on Geotechnique and Natural Hazards/3ième Conférence canadienne sur la géotechnique et les risques naturels. Edmonton, Alberta; CA; June 9–10 juin 2003. Canadian Geotechnical Society.

Baeten, N. J., Laberg, J. S., Forwick, M., Vorren, T. O., Vanneste, M., Forsberg, C. F., Kvalstad, T. J., & Ivanov, M. (2013). Morphology and origin of smaller-scale mass movements on the continental slope off northern Norway. *Geomorphology*, *187*, 122–134. https://doi.org/10.1016/j.geomorph.2013.01.008

Baeten, N. J., Laberg, J. S., Vanneste, M., Forsberg, C. F., Kvalstad, T. J., Forwick, M., Vorren, T. O., & Haflidason, H. (2014). Origin of shallow submarine mass movements and their glide planes—Sedimentological and geotechnical analyses from the continental slope off northern Norway. *Journal of Geophysical Research: Earth Surface*, *119*(11), 2335–2360. https://doi.org/10.1002/2013JF003068

Bøe, R., Bellec, V. K., Rise, L., Buhl-Mortensen, L., Chand, S., & Thorsnes, T. (2012). Catastrophic fluid escape venting-tunnels and related features associated with large submarine slides on the continental rise off Vesterålen-Troms. *North Norway. Marine and Petroleum Geology*, *38*(1), 95–103. https://doi.org/10.1016/j.marpetgeo.2012.08.008

Boyd, R., Williamson, P., & Haq, B. (1993). Seismic stratigraphy and passive-margin evolution of the southern exmouth plateau. *Sequence Stratigraphy and Facies Associations*, 579–603.

Bradley, K., Mallick, R., Andikagumi, H., Hubbard, J., Meilianda, E., Switzer, A., Du, N., Brocard, G., Alfian, D., Benazir, B., Feng, G., Yun, S.-H., Majewski, J., Wei, S., & Hill, E. M. (2019). Earthquake-triggered 2018 Palu Valley landslides enabled by wet rice cultivation. *Nature Geoscience*, *12*(11), 935–939. https://doi.org/10.1038/s41561-019-0444-1

Broussard, R. J. (2014). An Analysis of the Green Knoll Salt Dome, located in the Southeast Green Canyon, Deep Water Gulf of Mexico. University of New Orleans Theses and Dissertations. 1858.

Brown, A. R. (2011). Interpretation of three-dimensional seismic data. Society of Exploration Geophysicists and American Association of Petroleum Geologists.

Browne, G., Bull, S., Arnot, M., Boyes, A., King, P., & Helle, K. (2020). The role of mass transport deposits contributing to fluid escape: Neogene outcrop and seismic examples from north Taranaki, New Zealand. *Geo-Marine Letters*, *40*(5), 789–807. https://doi.org/10.1007/s00367-020-00641-z

Bryn, P., Berg, K., Forsberg, C. F., Solheim, A., & Kvalstad, T. J. (2005). Explaining the Storegga slide. *Marine and Petroleum Geology*, *22*(1), 11–19. https://doi.org/10.1016/j.marpetgeo.2004.12.003

Bull, S., Cartwright, J., & Huuse, M. (2009a). A review of kinematic indicators from mass-transport complexes using 3D seismic data. *Marine and Petroleum Geology*, *26*(7), 1132–1151. https://doi.org/10.1016/j.marpetgeo.2008.09.011

Bull, S., Cartwright, J., & Huuse, M. (2009b). A subsurface evacuation model for submarine slope failure. *Basin Research*, *21*(4), 433–443. https://doi.org/10.1111/j.1365-2117.2008.00390.x

Bull, S., Cartwright, J., & Huuse, M. (2009c). A subsurface evacuation-model for submarine slope failure. *Basin Research*, *21*(4), 433–443. https://doi.org/10.1111/j.1365-2117.2008.00390.x

Bünz, S., Mienert, J., Bryn, P., & Berg, K. (2005). Fluid flow impact on slope failure from 3D seismic data: A case study in the Storegga Slide. *Basin Research*, *17*(1), 109–122. https://doi.org/10.1111/j.1365-2117.2005.00256.x

Buss, C., Friedli, B., & Puzrin, A. M. (2019). Kinematic energy balance approach to submarine landslide evolution. *Canadian Geotechnical Journal*, *56*(9), 1351–1365. https://doi.org/10.1139/cgj-2017-0651

Carey, J., Crutchley, G. J., Mountjoy, J., Petley, D., McSaveney, M., & Lyndsell, B. (2019). Slow episodic movement driven by elevated pore-fluid pressures in shallow subaqueous slopes. *Geomorphology*, *329*, 99–107. https://doi.org/10.1016/j.geomorph.2018.12.034

Cartwright, J., & Santamarina, C. (2015). Seismic characteristics of fluid escape pipes in sedimentary basins: Implications for pipe genesis. *Marine and Petroleum Geology*, *65*, 126–140. https://doi.org/10.1016/j.marpetgeo.2015.03.023

Chaytor, J. D., Baldwin, W. E., Bentley, S. J., Damour, M., Jones, D., Maloney, J., Miner, M. D., Obelcz, J., & Xu, K. (2020). Short-and long-term movement of mudflows of the Mississippi River Delta Front and their known and potential impacts on oil and gas infrastructure. *Geological Society, London, Special Publications*, *500*(1), 587–604. https://doi.org/10.1144/SP500-2019-183

Chopra, S., & Marfurt, K. J. (2007). Seismic attributes for prospect identification and reservoir characterization. Society of Exploration Geophysicists and European Association of Geoscientists and Engineers.

Clare, M., Chaytor, J., Dabson, O., Gamboa, D., Georgiopoulou, A., Eady, H., Hunt, J., Jackson, C., Katz, O., Krastel, S., León, R., Micallef, A., Moernaut, J., Moriconi, R., Moscardelli, L., Mueller, C., Normandeau, A., Patacci, M., Steventon, M., … Jobe, Z. (2019). A consistent global approach for the morphometric characterization of subaqueous landslides. *Geological Society, London, Special Publications*, *477*(1), 455–477. https://doi.org/10.1144/SP477.15

Clari, P., Cavagna, S., Martire, L., & Hunziker, J. (2004). A Miocene mud volcano and its plumbing system: A chaotic complex revisited (Monferrato, NW Italy). *Journal of Sedimentary Research*, *74*(5), 662–676. https://doi.org/10.1306/022504740662

Couvin, B., Georgiopoulou, A., Mountjoy, J. J., Amy, L., Crutchley, G. J., Brunet, M., Cardona, S., Gross, F., Böttner, C., Krastel, S., & Pecher, I. (2020). A new depositional model for the Tuaheni Landslide Complex, Hikurangi Margin, New Zealand. *Geological Society, London, Special Publications*, *500*(1), 551–566. https://doi.org/10.1144/SP500-2019-180

Cruden, D. M., & Varnes, D. J. (1996). Landslides: investigation and mitigation. Chapter 3-Landslide types and processes. Transportation research board special report(247).

De Blasio, F. V., & Elverhoi, A. (2011). Properties of mass-transport deposits as inferred from dynamic modeling of subaqueous mass wasting: A short review. *Mass Transport Deposits in Deepwater Settings: SEPM Special Publication*, *96*, 499–508.

Deville, E., Scalabrin, C., Jouet, G., Cattaneo, A., Battani, A., Noirez, S., Vermesse, H., Olu, K., Corbari, L., Boulard, M., Marsset, T., Dall'Asta, M., Torelli, M., Pastor, L., Pierre, D., & Loubrieu, B. (2020). Fluid seepage associated with slope destabilization along the Zambezi margin (Mozambique). *Marine Geology*, *106275*. https://doi.org/10.1016/j.margeo.2020.106275

Dey, R., Hawlader, B., Phillips, R., & Soga, K. (2016). Numerical modelling of submarine landslides with sensitive clay layers. *Géotechnique*, *66*(6), 454–468. https://doi.org/10.1680/jgeot.15.P.111

Dutta, S., & Hawlader, B. (2019). Pipeline–soil–water interaction modelling for submarine landslide impact on suspended offshore pipelines. *Géotechnique*, *69*(1), 29–41. https://doi.org/10.1680/jgeot.17.P.084

Dykes, A. P., & Warburton, J. (2007). Mass movements in peat: A formal classification scheme. *Geomorphology*, *86*(1–2), 73–93. https://doi.org/10.1016/j.geomorph.2006.08.009

Elger, J., Berndt, C., Rüpke, L., Krastel, S., Gross, F., & Geissler, W. H. (2018). Submarine slope failures due to pipe structure formation. *Nature Communications*, *9*(1), 1–6. https://doi.org/10.1038/s41467-018-03176-1

Exon, N., Haq, B., & Von Rad, U. (1992). Exmouth Plateau revisited: scientific drilling and geological framework, Proceedings of the Ocean Drilling Program, Scientific Results. Ocean Drilling Program College Station, Tex, pp. 3-2.

Falvey, D., & Veevers, J. (1974). Physiography of the Exmouth and Scott plateaus, western Australia, and adjacent northeast Wharton Basin. *Marine Geology*, *17*(2), 21–59. https://doi.org/10.1016/0025-3227(74)90046-2

Fortin, A., Ouellet, D., Paradis, S., & Demers, D. (2008). Développement au Ministère des Transports du Québec d'un portail informatique pour l'accès à des bases de données géotechnique, Proceedings of the 4th Canadian Conference on Geohazards. From Causes to Management, Québec, Que, pp. 20-24

Geertsema, M., Blais-Stevens, A., Kwoll, E., Menounos, B., Venditti, J. G., Grenier, A., & Wiebe, K. (2018). Sensitive clay landslide detection and characterization in and around Lakelse Lake, British Columbia, Canada. *Sedimentary Geology*, *364*, 217–227. https://doi.org/10.1016/j.sedgeo.2017.12.025

Haq, B. U., Boyd, R. L., Exon, N. F., & von Rad, U. (1992). 47. Evolution of the central exmouth plateau: a post-drilling perspective1.

Hengesh, J., Dirstein, J. K., & Stanley, A. J. (2012). Seafloor geomorphology and submarine landslide hazards along the continental slope in the Carnarvon Basin, Exmouth Plateau, North West Shelf, Australia. *The APPEA Journal*, *52*(1), 493–512. https://doi.org/10.1071/AJ11039

Hengesh, J., Dirstein, J., & Stanley, A. (2013). Landslide geomorphology along the Exmouth plateau continental margin, North West Shelf, Australia. *Australian Geomechanics Journal*, *48*(4), 71–92.

Higgins, J. A., & Schrag, D. P. (2006). Beyond methane: Towards a theory for the Paleocene–Eocene thermal maximum[J]. *Earth and Planetary Science Letters*, *245*(3–4), 523–537.

Hong, Y., Wang, L., Ng, C. W., & Yang, B. (2017). Effect of initial pore pressure on undrained shear behaviour of fine-grained gassy soil. *Canadian Geotechnical Journal*, *54*(11), 1592–1600. https://doi.org/10.1139/cgj-2017-0015

Hull, J., & Griffiths, C. (2002). Sequence stratigraphic evolution of the Albian to Recent section of the Dampier Sub-basin, North West Shelf, Australia. PhD thesis 1999. University of Adelaide, Australia.

Hungr, O., Leroueil, S., & Picarelli, L. (2014). The Varnes classification of landslide types, an update. *Landslides*, *11*(2), 167–194. https://doi.org/10.1007/s10346-013-0436-y

Hustoft, S., Bünz, S., & Mienert, J. (2010). Three-dimensional seismic analysis of the morphology and spatial distribution of chimneys beneath the Nyegga pockmark field, offshore mid-Norway. *Basin Research*, *22*(4), 465–480. https://doi.org/10.1111/j.1365-2117.2010.00486.x

Huvenne, V. A., Croker, P. F., & Henriet, J. P. (2002). A refreshing 3D view of an ancient sediment collapse and slope failure. *Terra Nova*, *14*(1), 33–40. https://doi.org/10.1046/j.1365-3121.2002.00386.x

Jablonská, D., Di Celma, C. N., Alsop, G. I., & Tondi, E. (2018). Internal architecture of mass-transport deposits in basinal carbonates: A case study from southern Italy. *Sedimentology*, *65*(4), 1246–1276. https://doi.org/10.1111/sed.12420

Jackson, C. A. (2011). Three-dimensional seismic analysis of megaclast deformation within a mass transport deposit; implications for debris flow kinematics. *Geology*, *39*(3), 203–206. https://doi.org/10.1130/G31767.1

Keep, M., Harrowfield, M., & Crowe, W. (2007). The neogene tectonic history of the North West Shelf. *Australia. Exploration Geophysics*, *38*(3), 151–174. https://doi.org/10.1071/EG07022

Kvalstad, T. J., Andresen, L., Forsberg, C. F., Berg, K., Bryn, P., & Wangen, M. (2005). The Storegga slide: Evaluation of triggering sources and slide mechanics. *Marine and Petroleum Geology*, *22*(1), 245–256. https://doi.org/10.1016/j.marpetgeo.2004.10.019

Laberg, J., & Vorren, T. (2000). The Trænadjupet Slide, offshore Norway—morphology, evacuation and triggering mechanisms. *Marine Geology*, *171*(1–4), 95–114. https://doi.org/10.1016/S0025-3227(00)00112-2

Lacroix, P., Handwerger, A. L., & Bièvre, G. (2020). Life and death of slow-moving landslides. *Nature Reviews Earth & Environment*. https://doi.org/10.1038/s43017-020-0072-8

Lambe, T. W., & Whitman, R. V. (1969). *Soil mechanics* (p. 553). John Wiley.

Lee, S., & Chough, S. (2001). High-resolution (2–7 kHz) acoustic and geometric characters of submarine creep deposits in the South Korea Plateau, East Sea. *Sedimentology*, *48*(3), 629–644. https://doi.org/10.1046/j.1365-3091.2001.00383.x

Legget, R. F., & LaSalle, P. (1978). Soil studies at Shipshaw, Quebec: 1941 and 1969. *Canadian Geotechnical Journal*, *15*(4), 556–564. https://doi.org/10.1139/t78-059

Li, W., Alves, T. M., Urlaub, M., Georgiopoulou, A., Klaucke, I., Wynn, R. B., Gross, F., Meyer, M., Repschläger, J., Berndt, C., & Krastel, S. (2017). Morphology, age and sediment dynamics of the upper headwall of the Sahara Slide Complex, Northwest Africa: Evidence for a large Late Holocene failure. *Marine Geology*, *393*, 109–123. https://doi.org/10.1016/j.margeo.2016.11.013

Li, W., Alves, T. M., Wu, S., Rebesco, M., Zhao, F., Mi, L., & Ma, B. (2016). A giant, submarine creep zone as a precursor of large-scale slope instability offshore the Dongsha Islands (South China Sea). *Earth and Planetary Science Letters*, *451*, 272–284. https://doi.org/10.1016/j.epsl.2016.07.007

Locat, A., Leroueil, S., Bernander, S., Demers, D., Jostad, H. P., & Ouehb, L. (2011). Progressive failures in eastern Canadian and Scandinavian sensitive clays. *Canadian Geotechnical Journal*, *48*(11), 1696–1712. https://doi.org/10.1139/t11-059

Locat, A., Leroueil, S., Fortin, A., Demers, D., & Jostad, H. P. (2015). The 1994 landslide at Sainte-Monique, Quebec: Geotechnical investigation and application of progressive failure analysis. *Canadian Geotechnical Journal*, *52*(4), 490–504. https://doi.org/10.1139/cgj-2013-0344

Locat, A., Locat, P., Demers, D., Leroueil, S., Robitaille, D., & Lefebvre, G. (2017). The Saint-Jude landslide of 10 May 2010, Quebec, Canada: Investigation and characterization of the landslide and its failure mechanism. *Canadian Geotechnical Journal*, *54*(10), 1357–1374. https://doi.org/10.1139/cgj-2017-0085

Løseth, H., Wensaas, L., Arntsen, B., Hanken, N.-M., Basire, C., & Graue, K. (2011). 1000 m long gas blow-out pipes. *Marine and Petroleum Geology*, *28*(5), 1047–1060.

Løvholt, F., Bondevik, S., Laberg, J. S., Kim, J., & Boylan, N. (2017). Some giant submarine landslides do not produce large tsunamis. *Geophysical Research Letters*, *44*(16), 8463–8472. https://doi.org/10.1002/2017GL074062

Madhusudhan, B., Clare, M., Clayton, C., & Hunt, J. (2017). Geotechnical profiling of deep-ocean sediments at the AFEN submarine slide complex. *Quarterly Journal of Engineering Geology and Hydrogeology*, *50*(2), 148–157. https://doi.org/10.1144/qjegh2016-057

Maher, B. A., & Thompson, R. (Eds.) (1999). *Quaternary climates, environments and magnetism*. Cambridge University Press. https://doi.org/10.1017/CBO9780511535635

Masson, D., Harbitz, C., Wynn, R., Pedersen, G., & Løvholt, F. (2006). Submarine landslides: Processes, triggers and hazard prediction. *Philosophical Transactions of the Royal Society A: Mathematical, Physical and Engineering Sciences*, *364*(1845), 2009–2039. https://doi.org/10.1098/rsta.2006.1810

Micallef, A., Masson, D. G., Berndt, C., & Stow, D. A. (2007). Morphology and mechanics of submarine spreading: A case study from the Storegga Slide. *Journal of Geophysical Research: Earth Surface*, *112*(F3). https://doi.org/10.1029/2006JF000739

Micallef, A., Masson, D. G., Berndt, C., & Stow, D. A. (2009). Development and mass movement processes of the north-eastern Storegga Slide. *Quaternary Science Reviews*, *28*(5–6), 433–448. https://doi.org/10.1016/j.quascirev.2008.09.026

Micallef, A., Mountjoy, J. J., Krastel, S., Crutchley, G., & Koch, S. (2016). Shallow gas and the development of a weak layer in submarine spreading, Hikurangi margin (New Zealand), Submarine Mass Movements and their Consequences. Springer, 419–426.

Moss, J., & Cartwright, J. (2010). 3D seismic expression of km-scale fluid escape pipes from offshore Namibia. *Basin Research*, *22*(4), 481–501. https://doi.org/10.1111/j.1365-2117.2010.00461.x

Nemec, W. (1990). Aspects of sediment movement on steep delta slopes. *Coarse-grained Deltas*, *10*, 29–73.

Nugraha, H. D., Jackson, C.- A.-L., Johnson, H. D., Hodgson, D. M., & Clare, M. (2019). How erosive are submarine landslides?

Nugraha, H. D., Jackson, C. A. L., Johnson, H. D., Hodgson, D. M., & Reeve, M. T. (2018). Tectonic and oceanographic process interactions archived in Late Cretaceous to Present deep-marine stratigraphy on the Exmouth Plateau, offshore NW Australia. *Basin Research*.

Odenstad, S. (1952). The landslide at Sköttorp on the Lidan River, February 2, 1946. R. Swedish Inst. Proc., 1951, 4, 1–38.

Ogata, K., Mountjoy, J., Pini, G. A., Festa, A., & Tinterri, R. (2014). Shear zone liquefaction in mass transport deposit emplacement: A multi-scale integration of seismic reflection and outcrop data. *Marine Geology*, *356*, 50–64. https://doi.org/10.1016/j.margeo.2014.05.001

Paull, C., Ussler, W., & Holbrook, W. (2007). Assessing methane release from the colossal Storegga submarine landslide. *Geophysical Research Letters*, *34*(4). https://doi.org/10.1029/2006GL028331

Plaza-Faverola, A., Bünz, S., & Mienert, J. (2011). Repeated fluid expulsion through sub-seabed chimneys offshore Norway in response to glacial cycles. *Earth and Planetary Science Letters*, *305*(3–4), 297–308. https://doi.org/10.1016/j.epsl.2011.03.001

Pope, E. L., Talling, P. J., & Carter, L. (2017). Which earthquakes trigger damaging submarine mass movements: Insights from a global record of submarine cable breaks? *Marine Geology*, *384*, 131–146. https://doi.org/10.1016/j.margeo.2016.01.009

Posamentier, H. W., & Martinsen, O. J. (2011). The character and genesis of submarine mass-transport deposits: insights from outcrop and 3D seismic data. Mass-transport deposits in deepwater settings. *Society for Sedimentary Geology (SEPM) Special Publication*, *96*, 7-38.

Principaud, M., Mulder, T., Gillet, H., & Borgomano, J. (2015). Large-scale carbonate submarine mass-wasting along the northwestern slope of the Great Bahama Bank (Bahamas): Morphology, architecture, and mechanisms. *Sedimentary Geology*, *317*, 27–42. https://doi.org/10.1016/j.sedgeo.2014.10.008

Randolph, M. F., & White, D. J. (2012). Interaction forces between pipelines and submarine slides—A geotechnical viewpoint. *Ocean Engineering*, *48*, 32–37. https://doi.org/10.1016/j.oceaneng.2012.03.014

Roberts, K., Davies, R., & Stewart, S. (2010). Structure of exhumed mud volcano feeder complexes, Azerbaijan. *Basin Research*, *22*(4), 439–451. https://doi.org/10.1111/j.1365-2117.2009.00441.x

Savage, W. Z., & Varnes, D. J. (1987). Mechanics of gravitational spreading of steep-sided ridges («sackung»). *Bulletin of the International Association of Engineering Geology*, *35*(1), 31–36. https://doi.org/10.1007/BF02590474

Sawyer, D. E., Flemings, P. B., Dugan, B., & Germaine, J. T. (2009). Retrogressive failures recorded in mass transport deposits in the Ursa Basin, Northern Gulf of Mexico. *Journal of Geophysical Research: Solid Earth*, *114*(B10). https://doi.org/10.1029/2008JB006159

Sawyer, D. E., & Hodelka, B. (2016). Tiny fossils, big impact: The role of foraminifera-enriched condensed section in arresting the movement of a large retrogressive submarine landslide in the Gulf of Mexico, Submarine Mass Movements and their Consequences. Springer, 479–486.

Scarselli, N., McClay, K., & Elders, C. (2013). Submarine slide and slump complexes, Exmouth Plateau, NW Shelf of Australia, The Sedimentary Basins of Western Australia IV. Proceedings of the Petroleum Exploration Society of Australia SymposiumPerth, WA.

Scarselli, N., McClay, K., & Elders, C. (2019). Seismic Examples of Composite Slope Failures (Offshore North West Shelf, Australia). Submarine Landslides: Subaqueous Mass Transport Deposits from Outcrops to Seismic Profiles. 261-276.

Shillington, D. J., Seeber, L., Sorlien, C. C., Steckler, M. S., Kurt, H., Dondurur, D., Cifci, G., Imren, C., Cormier, M.-H., McHugh, C. M. G., Gurcay, S., Poyraz, D., Okay, S., Atgin, O., & Diebold, J. B. (2012). Evidence for widespread creep on the flanks of the Sea of Marmara transform basin from marine geophysical data. *Geology*, *40*(5), 439–442. https://doi.org/10.1130/G32652.1

Silva, A. J., & Booth, J. S. (1984). Creep behavior of submarine sediments. *Geo-marine Letters*, *4*(3–4), 215–219. https://doi.org/10.1007/BF02281709

Sobiesiak, M. S., Kneller, B., Alsop, G. I., & Milana, J. P. (2018). Styles of basal interaction beneath mass transport deposits. *Marine and Petroleum Geology*, *98*, 629–639. https://doi.org/10.1016/j.marpetgeo.2018.08.028

Strasser, M., Kölling, M., Ferreira, C. D. S., Fink, H. G., Fujiwara, T., Henkel, S., Ikehara, K., Kanamatsu, T., Kawamura, K., Kodaira, S., Römer, M., & Wefer, G. (2013). A slump in the trench: Tracking the impact of the 2011 Tohoku-Oki earthquake. *Geology*, *41*(8), 935–938. https://doi.org/10.1130/G34477.1

Sun, Q., Cartwright, J., Wu, S., & Chen, D. (2013). 3D seismic interpretation of dissolution pipes in the South China Sea: Genesis by subsurface, fluid induced collapse. *Marine Geology*, *337*, 171–181. https://doi.org/10.1016/j.margeo.2013.03.002

Tappin, D. (2010). Submarine mass failures as tsunami sources: Their climate control. *Philosophical Transactions of the Royal Society A: Mathematical, Physical and Engineering Sciences*, *368*(1919), 2417–2434. https://doi.org/10.1098/rsta.2010.0079

Thomas, S., Hooper, J., & Clare, M. (2010). Constraining geohazards to the past: Impact assessment of submarine mass movements on seabed developments, Submarine mass movements and their consequences. Springer, 387–398.

Urlaub, M., Talling, P. J., & Masson, D. G. (2013). Timing and frequency of large submarine landslides: Implications for understanding triggers and future geohazard. *Quaternary Science Reviews*, *72*, 63–82. https://doi.org/10.1016/j.quascirev.2013.04.020

Urlaub, M., Talling, P. J., Zervos, A., & Masson, D. (2015). What causes large submarine landslides on low gradient (< 2°) continental slopes with slow (~ 0.15 m/kyr) sediment accumulation? *Journal of Geophysical Research: Solid Earth*, *120*(10), 6722–6739.

Varnes, D. J. (1978). Slope movement types and processes. *Special Report*, *176*, 11–33.

Velayatham, T., Holford, S. P., & Bunch, M. A. (2018). Ancient fluid flow recorded by remarkably long, buried pockmark trains observed in 3D seismic data, Exmouth Plateau, Northern Carnarvon basin. *Marine and Petroleum Geology*, *95*, 303–313. https://doi.org/10.1016/j.marpetgeo.2018.05.007

Velayatham, T., Holford, S., Bunch, M., King, R., & Magee, C. (2019). 3D Seismic Analysis of Ancient Subsurface Fluid Flow in the Exmouth Plateau, Offshore Western Australia.

von Rad, U., Haq, B. U. et al (1992). Proceedings of the Ocean Program, Scientific Results. Ocean Drilling Program, Leg 122.

Watkinson, I. M., & Hall, R. (2019). Impact of communal irrigation on the 2018 Palu earthquake-triggered landslides. *Nature Geoscience*, *12*(11), 940–945. https://doi.org/10.1038/s41561-019-0448-x

Watson, P., Bransby, F., Delimi, Z. L., Erbrich, C., Randolph, M., Rattley, M., Silva, M., Stevens, B., Thomas, S., & Westgate, Z. (2019). Foundation design in offshore carbonate sediments–building on

knowledge to address future challenges, From Research to Applied Geotechnics: Invited Lectures of the XVI Pan-American Conference on Soil Mechanics and Geotechnical Engineering (XVI PCSMGE). 17-20 November 2019, Cancun, Mexico. IOS Press, pp. 240.

Watts, P., Grilli, S. T., Tappin, D. R., & Fryer, G. J. (2005). Tsunami generation by submarine mass failure. II: Predictive equations and case studies. *Journal of Waterway, Port, Coastal, and Ocean Engineering*, *131*(6), 298–310. https://doi.org/10.1061/(ASCE)0733-950X(2005)131:6(298)

Wu, N., Jackson, C. A., Johnson, H., & Hodgson, D. M. (2019). Lithological, petrophysical and seal properties of mass-transport complexes (MTCs), northern Gulf of Mexico. EarthArXiv. February, 19.

Yang, J., Davies, R. J., & Huuse, M. (2013). Gas migration below gas hydrates controlled by mass transport complexes, offshore Mauritania. *Marine and Petroleum Geology*, *48*, 366–378. https://doi.org/10.1016/j.marpetgeo.2013.09.003

Zakeri, A. (2009). Review of state-of-the-art: Drag forces on submarine pipelines and piles caused by landslide or debris flow impact. *Journal of Offshore Mechanics and Arctic Engineering*, *131*(1), 2957922. https://doi.org/10.1115/1.2957922

Zhu, H., & Randolph, M. F. (2010). Large deformation finite-element analysis of submarine landslide interaction with embedded pipelines. *International Journal of Geomechanics*, *10*(4), 145–152. https://doi.org/10.1061/(ASCE)GM.1943-5622.0000054

**How to cite this article:** Wu N, Jackson CA-L, Johnson HD, et al. The formation and implications of giant blocks and fluid escape structures in submarine lateral spreads. *Basin Res*. 2021;33:1711–1730. https://doi.org/10.1111/bre.12532